OPTIMIZING TIME RESOLVED PHOSPHORIMETRY

BY

CHARLES GLENN BARNES

A DISSERTATION PRESENTED TO THE GRADUATE COUNCIL
OF THE UNIVERSITY OF FLORIDA IN
PARTIAL FULFILLMENT OF THE REQUIREMENTS
FOR THE DEGREE OF DOCTOR OF PHILOSOPHY

UNIVERSITY OF FLORIDA
1980

ACKNOWLEDGEMENTS

I wish to first express my belief in the guidance of Jesus Christ in my life, and in my career. In addition, I would like to take this opportunity to express my gratitude to those people who have assisted me in this endeavor. To my research director, Dr. James D. Winefordner, go my appreciation and thanks for his patience and support, and for his willingness to make himself readily accessible to students. To Dr. John Legg of Mississippi College go my sincere thanks for his friendship and guidance, and for the example that he sets for myself and other students.

I would like to express my loving gratitude to my wife, Joyce, who continued to love me even through the ultimate test of a marriage -- the writing of a dissertation; and to my parents and family who have contributed their love and financial support for these 25 years. Many thanks to my friends at the Baptist Student Center for making me a part of your fellowship.

Thanks are due to Art Grant and the Machine Shop gang for their artistry, and to the JDW group for their knowledge and the willingness to share it.

TABLE OF CONTENTS

Page

ACKNOWLEDGEMENTS ---------------------------------- ii

LIST OF TABLES ------------------------------------ iv

LIST OF FIGURES ----------------------------------- v

ABSTRACT -- vii

CHAPTER

I. INTRODUCTION ----------------------------------- 1

Historical -- 1
Time Resolved Phosphorimetry ---------------------- 5

II. THEORETICAL CONSIDERATIONS -------------------- 28

Kinetic Analysis of Molecular Processes ----------- 28
Intensity Expressions ----------------------------- 30
Response Profiles --------------------------------- 61
Summary --- 100

III. EXPERIMENTAL --------------------------------- 102

Instrumentation ----------------------------------- 102
Reagents -- 112
Instrumental Procedure ---------------------------- 113
Sampling Procedure -------------------------------- 114

IV. RESULTS AND DISCUSSION ------------------------ 118

Validation of Theoretical Analysis ---------------- 118
Time Resolution of Phosphor Mixtures -------------- 141

V. CONCLUSIONS ------------------------------------ 155

APPENDIX -- 157

LIST OF REFERENCES -------------------------------- 164

BIOGRAPHICAL SKETCH ------------------------------- 167

LIST OF TABLES

TABLE Page

1. FINAL WORKING EQUATIONS FOR THE EXPONENTIAL METHOD OF TIME RESOLUTION FOR A BINARY MIXTURE ---------------------------------- 24
2. FINAL WORKING EQUATIONS FOR THE EXPONENTIAL METHOD OF TIME RESOLUTION FOR A TERNARY MIXTURE ---------------------------------- 25
3. DEFINITION OF PARAMETERS ------------------- 38
4. KEY TO GATE WIDTH FOR FIGURES 5-7 ---------- 51
5. PARAMETERS FOR RESPONSE PROFILES ----------- 63
6. EXPERIMENTAL EQUIPMENT AND MANUFACTURERS ---- 105
7. PRELIMINARY LIFETIME MEASUREMENTS ----------- 119
8. PARAMETERS FOR EXPERIMENTAL VALIDATION ------ 121
9. COMPARISON OF THEORETICAL AND EXPERIMENTAL INTENSITY RATIOS FOR THIORIDAZINE HCl ------ 125
10. COMPARISON OF THEORETICAL AND EXPERIMENTAL INTENSITY RATIOS FOR VANILLIN ------------- 126
11. COMPARISON OF THEORETICAL AND EXPERIMENTAL INTENSITY RATIOS FOR NUPERCAINE HCl--------- 127
12. AVERAGE RESULTS OF INTENSITY MEASUREMENTS FOR THREE PHOSPHORS -------------------------- 128
13. ANALYSIS OF BINARY MIXTURE I --------------- 147
14. ANALYSIS OF BINARY MIXTURE II -------------- 149
15. ANALYSIS OF TERNARY MIXTURE I -------------- 152

A1. KINETIC EVENTS IN A RIGID GLASS SYSTEM CONTAINING ONE SOLUTE --------------------- 158

LIST OF FIGURES

Figure Page

1. Schematic diagram and molecular electronic and vibrational energy levels ------------------ 7
2. Schematic representation of the operation of a pulsed source gated phosphorimeter ------- 15
3. Schematic representation of the excitation process with a pulsed source --------------- 35
4. A typical relative response profile --------- 47
5. Optimum delay versus lifetime (f = 1 Hz) ---- 53
6. Optimum delay versus lifetime (f = 10 Hz) --- 55
7. Optimum delay versus lifetime (f = 50 Hz) --- 57
8. Response profile (t_g = 5×10^{-3}s, f = 1 Hz) --- 65
9. Response profile (t_g = 5×10^{-3}s, f = 10 Hz) -- 67
10. Response profile (t_g = 5×10^{-3}s, f = 50 Hz) -- 69
11. Response profile (t_g = 5×10^{-3}s, f = 100 Hz)-- 71
12. Response profile (t_g = 5×10^{-4}s, f = 1 Hz)---- 73
13. Response profile (t_g = 5×10^{-4}s, f = 10 Hz)--- 75
14. Response profile (t_g = 5×10^{-4}s, f = 50 Hz)--- 77
15. Response profile (t_g = 5×10^{-4}s, f = 100 Hz)-- 79
16. Response profile (t_g = 5×10^{-5}s, f = 1 Hz)---- 81
17. Response profile (t_g = 5×10^{-5}s, f = 10 Hz)--- 83
18. Response profile (t_g = 5×10^{-5}s, f = 50 Hz)--- 85
19. Response profile (t_g = 5×10^{-5}s, f = 100 Hz)-- 87

20. Schematic representation of phosphorescence growth during the excitation pulse for two phosphors with different lifetimes ---------- 92

21. Schematic representation of the effect of gate width on observed phosphorescence signal -- 95

22. Schematic representation of the effect of frequency on pulse-to-pulse phosphorescence intensity growth ---------------------------- 98

23. Block diagram of the experimental system ----- 104

24. Growth profile for thioridazine HCl at 1 Hz -- 132

25. Growth profile for thioridazine HCl at 10 Hz - 134

26. Growth profile for thioridazine HCl at 100 Hz- 136

27. Growth profile for nupercaine HCl at 10 Hz --- 138

28. Growth profile for nupercaine HCl at 100 Hz -- 140

A1. Kinetic processes occurring during growth and decay of phosphorescence ------------------- 160

Abstract of Dissertation Presented to the Graduate Council
of the University of Florida in Partial Fulfillment of the
Requirements for the Degree of Doctor of Philosophy

OPTIMIZING TIME RESOLVED PHOSPHORIMETRY

By

Charles Glenn Barnes

December, 1980

Chairman: James Dudley Winefordner
Major Department: Chemistry

Time resolved phosphorimetry (TRP) is an analytical method with primary application to analysis of multicomponent mixtures of spectrally similar species. The resolution of such a mixture is attained by utilizing differences in the phosphorescence decay lifetimes (τ) of the mixture components. Earlier work has relied heavily upon multichannel detection systems which scan the entire emission decay curve as a function of time. However, a phosphorimeter incorporating a pulsed excitation source with a single channel gated detection system (boxcar averager or integrator) has several characteristics that make it attractive for TRP. These include relatively low cost and flexibility in selection of the operating parameters of gate width (t_g), delay time (t_d), pulse repetition rate (f), and integration time constant. This flexibility should allow resolution of mixtures over a large range of phosphorescence lifetimes.

In this work, the potential for applying such a system to TRP is examined. Theoretical expressions are derived which demonstrate the relationships of observed phosphorescence intensity on the phosphorescence lifetime and on the characteristic parameters of the experimental system. Plots of relative response versus lifetime under various sets of parameters are presented and are used to predict and interpret the effect of excitation peak width, t_g, t_d, f, and τ on the observed signal level. At a fixed set of parameters, there is a lifetime to which the system has optimum response, τ_{max}. An expression is presented which allows positioning this maximum at any selected lifetime.

A pulsed-laser source boxcar averager phosphorimeter is described. Experimental results are presented to demonstrate the validity of the theoretical expressions. The expressions are used to optimize the experimental system for TRP analysis of binary and ternary mixtures of spectrally similar species. Results indicate that this type of analysis requires a mixture with two or three components, the lifetimes of which differ by a factor of two or more. The major errors are due to photodecomposition of the samples and excessive source flicker noise.

CHAPTER I
INTRODUCTION

Historical

Phosphorimetry was first proposed as a method of chemical analysis by Lewis and Kasha (1). They reviewed the little that was known about phosphorescence at that time, and based upon their own research, wrote "for every substance, there is a unique phosphorescent state" (p.2102). Further, they ascribed phosphorescence to the triplet state of the unsaturated molecule. The next significant work on phosphorimetry was that of Keirs, Britt and Wentworth thirteen years later (2), which first demonstrated the enormous potential of phosphorimetry for chemical analysis. The authors discussed the experimental and theoretical aspects of phosphorimetry and demonstrated that binary mixtures of phosphors could be spectrally resolved by judicious selection of excitation and emission wavelengths. For mixtures of phosphors whose excitation and emission spectra were similar, they used a technique called "phosphoroscopic resolution," which resolved the components by utilizing differences in their phosphorescence decay rates. The technique was applicable to phosphors having lifetimes in the millisecond region.

O'Haver and Winefordner in 1966 discussed the influence of mechanical phosphoroscope design on the detected phosphorescence intensity (3). Expressions were derived which related the measured and instantaneous phosphorescence intensity to the decay time of the phosphorescent species and to the characteristic parameters of the phosphoroscope used in the measurement system. Numerical results were given for two different phosphoroscopes. The expressions were later extended (4) to apply to pulsed sources and gated detection systems, specifically, to a pulsed flash tube and a pulsed photomultiplier tube, using an average-reading DC meter for output. They were able to predict the "sample-to-interferent ratio enhancement" under differing sets of experimental conditions, based upon the relative lifetimes of the analyte and interferent.

St. John and Winefordner (5) published the results of a study on "Time Resolved Phosphorimetry," in which binary mixtures of phosphors were resolved based upon differences in lifetime. The method employed a CW source and a DC readout system coupled with a logarithmic converter to display log-phosphorescence intensity versus time, following the cessation of excitation via a manual guillotine shutter. Hollifield and Winefordner (6) designed a unique single-disk phosphorimeter to measure intensity at small intervals along the emission decay curve and used it to time resolve several binary mixtures. The overall error was found to be largest when the lifetimes of the components were similar, or when one component was present in great excess.

Winefordner suggested the potential advantages of utilizing a pulsed source fast (gated) readout system for time resolved phosphorimetry (7). Fisher and Winefordner (8) built such a system and applied it to the analysis of binary and ternary mixtures of phosphors. The system was designed primarily for rapidly decaying $n-\pi^*$ phosphors and utilized a pulsed flash tube for excitation and a multichannel signal averager coupled to a logarithmic converter for output. Expressions were derived which related measured phosphorescence signal to the concentration of each analyte (phosphor) in a multi-component mixture of spectrally similar organic molecules. Three specific methods of data reduction were described and employed for estimating concentrations from phosphorescence signals measured at different times after the termination of excitation. O'Donnell et al. (9) modified the Fisher phosphorimeter by using a higher powered xenon flashlamp and a rotating sample cell, and quantitated mixtures of halogenated biphenyls. Harbaugh, O'Donnell, and Winefordner measured phosphorimetric lifetimes and qualitatively and quantitatively identified drug mixtures with this system (10,11).

Wilson and Miller (12) described a versatile computer-controlled laser phosphorimeter. The phosphorescence spectra were recorded on magnetic tape as a family of signal averaged decay curves. The system would average one hundred decay curves at 1 nm intervals over a 150-200 nm range. The technique of component-resolved spectrometry was discussed in detail and illustrated by resolution of the phosphorescence spectra of a binary mixture. The data reduction involved a non-linear least squares fit in n-dimensional space (12,13).

O'Donnell and Winefordner (14) reviewed advances in instrumentation and methodology for phosphorimetry, and discussed the potential of the pulsed source gated detection system over standard systems. Goeringer and Pardue (15) designed a silicon intensified-target vidicon (SIT) camera for phosphorescence studies and described applications to room temperature phosphorimetry of salts of organic acids. The spectral decay data were processed by a variety of regression methods, which were based in part upon the work of Ridder and Margerum (16), Mieling and Pardue (17), and Willis et al. (18) on simultaneous kinetic analysis. In addition, the authors applied the internal standard method to phosphorimetry for the first time and reduced overall imprecision by two to five times. Boutilier and Winefordner (19) described a laser-source time resolved phosphorimeter and applied it to investigating the external heavy atom effect on the phosphorescence lifetimes, relative intensities, and limits of detection of drugs.

Time Resolved Phosphorimetry

Phosphorescence is the long-lived luminescence observed following excitation of some types of molecules with an external light source. The physical basis for phosphorescence can be seen in Figure 1, which is a schematic diagram of the processes taking place during excitation/emission of molecular luminescence (2,20). Absorption of a photon (A) excites the molecule to some vibrational level of an excited singlet state (10^{-15}s). (Absorption to a triplet state is extremely unlikely, because the transition is spin-forbidden.) Usually, the first excited singlet, S_1, is the state that is optically pumped, but not always. Within the electronic state thus populated, vibrational relaxation (VR) (plus solvent-relaxation), efficiently deactivates the molecule to the lowest vibrational level of that electronic state (10^{-13}s). Further deactivation to a lower electronic level occurs by internal conversion (IC), which is a nonradiative relaxation to a lower electronic state of the same multiplicity (10^{-12}s). Once the molecule is in the S_1 state, further deactivation can occur by further internal conversion to the ground state. However, because the energy gap between S_0 and S_1 is usually larger than that between the higher electronic states, the process is less efficient, and a

Figure 1. Schematic diagram of molecular electronic and vibrational energy levels.

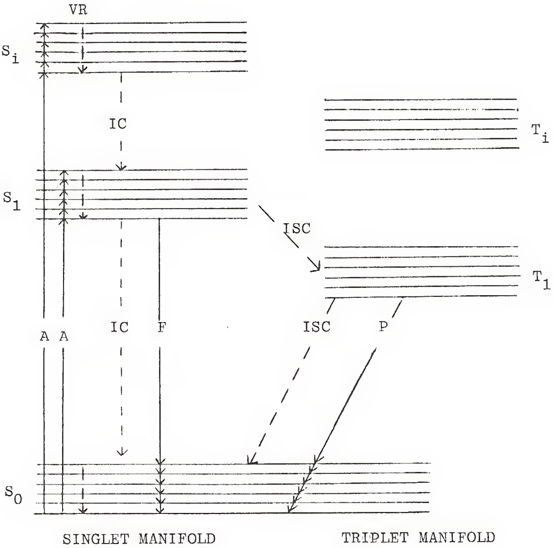
VR
S_i
IC
T_i
S_1
ISC
T_1
A A
IC
F
ISC
P
S_0
SINGLET MANIFOLD
TRIPLET MANIFOLD

spin-allowed radiative transition, fluorescence (F), can compete effectively for depopulation of the S_1 state.

There is, however, another pathway for de-excitation of the S_1 state. Due to spin-orbital coupling, the less energetic T_1 state can be populated from the S_1 state. This nonradiative process, occurring between states of differing multiplicity, is intersystem crossing (ISC). The efficiency of ISC varies greatly from molecule to molecule, and is extremely dependent upon the molecular environment.

The T_1 state can be depopulated by further ISC to the ground state singlet, or by a spin-forbidden radiative transition, $T_1 \rightarrow S_0$. This spin-forbidden radiative transition between states of different multiplicity is phosphorescence (P). The probability of a spin-forbidden transition is 10^{-3} to 10^{-6} smaller than that of the corresponding spin-allowed transition. Therefore, the mean lifetime of the T_1 state is usually 10^{-3}s to several seconds in duration, while the mean lifetime of the S_1 state is approximately 10^{-8}s.

Observation of molecular luminescence requires that the radiative processes compete effectively with the non-radiative processes for depopulation of the excited states. Therefore, molecules possessing rigid molecular skeletons and large separations between the ground state and lowest excited states most often exhibit fluorescence/phosphorescence (20). Note that the two luminescence processes compete indirectly for depopulation of the T_1 state. Aromatic molecules, possessing rigid-ring structures, form the largest class of compounds to exhibit luminescence.

Due to the long lifetime of the triplet state, many other processes compete with phosphorescence for depopulation of the triplet. These include collisional deactivation by solvent molecules; quenching by paramagnetic species, especially oxygen; and photochemical processes. For this reason, phosphorescence is normally observed with the phosphorescent species (phosphor) frozen rigidly into a solvent matrix at or below liquid nitrogen temperatures (77 K). This minimizes collisional processes (20).

The instrument used to measure phosphorescence is known as a phosphorimeter. The sample is irradiated with a suitable source, and the phosphorescence is usually observed at 90° to the excitation axis. Because phosphorescence has a longer lifetime (i.e., persists for a longer time following termination of excitation) than scatter and fluorescence, phosphorescence can be measured without interference from either process by using an experimental system that excites the sample for some period of time, stops the excitation, and waits for fluorescence and scatter to disappear before making the intensity measurement (14). Normally, a mechanical shutter system (phosphoroscope) is employed, but pulsed systems have been applied to advantage (8-11,21).

In order for phosphorescence to be used for quantitative chemical analysis, there must be a well-defined relationship between analyte concentration and observed phosphorescence intensity. An approximate relationship is given by Equation (1), which assumes a dilute solution of the analyte, monochromatic radiation, and no prefilter or postfilter effects:

$$P_p = P_0 \, 2.3 \text{ abc } Y_p \qquad (1)$$

In Equation (1), P_p is defined to be the radiant phosphorescence power (W) emitted under a given set of experimental conditions, Y_p is the power efficiency (ratio of radiant power emitted to radiant flux absorbed), a is the molar absorptivity (L $\text{mole}^{-1}\text{cm}^{-1}$), b is the absorption path length (cm), and c is the molar concentration of the absorber (mole L^{-1}). The approximation (2.3 abc) < 0.05 is required for this linear relationship to be valid, and is normally met at the low concentration levels encountered in analytical phosphorimetry. This expression is strictly valid only when the excitation and emission have reached steady state (21,22,23).

Conventional phosphorimetry, as an analytical method, exhibits excellent sensitivity, low limits of detection, and large linear dynamic ranges for many phosphors. Selectivity is inherent in the nature of phosphorimetry; both the excitation and emission wavelengths can be varied to selectively excite/monitor the phosphorescence due to one particular species. The principal value of phosphorimetry was pointed out by O'Donnell and Winefordner in 1975 in a review article on phosphorimetry in clinical analysis. They stated:

> the greatest use of phosphorimetry in the clinical laboratory will not be for the analysis of very large numbers of samples for one species via automatic instrumentation, but rather will be for the analysis of those species impossible to measure by conventional methods. . . . (14, p. 285)

This statement summarizes quite well the contribution of phosphorimetry towards analytical chemistry as a whole.

Although phosphorimetric analysis does have a high degree of inherent selectivity, cases obviously arise in which interfering phosphors cannot be adequately minimized by spectral resolution. Molecular emission bands are quite broad, and so spectral overlap occurs frequently. Increased selectivity is required to solve this problem, and the additional selectivity is achieved in the time domain.

The observed phosphorescence intensity following an excitation pulse decays away slowly. In most cases, the shape of the "emission decay curve" is an exponential function, with the intensity at any time, t, given by

$$I = I_0 \exp\ (-t/\tau) \qquad (2)$$

where I is the observed phosphorescence intensity at time t, I_0 is the initial (t = 0) intensity, and τ is the phosphorescence decay lifetime(s). In this work, τ or "lifetime" will refer exclusively to the experimentally observed phosphorescence decay lifetime. Any other type of lifetime will be distinguished from τ by a subscript or superscript.

The experimental lifetime is a function of both the specific molecule (phosphor) and the specific environment and temperature. Fortunately, it does not vary greatly with temperature in the vicinity of 77 K. Neither does τ show substantial variation with concentration over a limited concentration range, although changes in the solvent system, or even in the sampling/freezing process, can cause τ to vary. However, for one specific set of experimental conditions, τ is characteristic of the particular molecule under study, and is independent of analyte concentration in dilute solutions (7,21,24).

Phosphors tend to fall into two relatively distinct categories with regard to lifetime. Molecules involving an $n \rightarrow \pi^*$ transition (carbonyls, thiocarbonyls, and some azo compounds) tend to have lifetimes on the order of milliseconds. Those involving $\pi \rightarrow \pi^*$ transitions typically exhibit lifetimes ranging from tenths of a second to tens of seconds (25). The entire range of phosphorescence lifetimes is thus approximately 10^{-4}s to 10 s. The probability of two different phosphors in a sample mixture possessing identical excitation maxima, emission maxima, and lifetimes is small, although this does occur. Resolution of spectrally similar phosphors based upon differences in phosphorescence lifetime is known as time resolved phosphorimetry (TRP). TRP is of value when instrumental or spectroscopic methods for resolution fail, or are not available; and if prior chemical treatment of the sample would not effect the desired separation, would result in lengthy analysis, or would introduce contamination (21).

Conventional mechanical shutter phosphorimeters do not have the versatility required for application to TRP. Instead, a pulsed source gated detection system (which has advantages even for conventional phosphorimetry) is required.

A pulsed source TRP system employing a conventional single channel ("boxcar" averager or integrator) measurement system is shown schematically in Figure 2 (4). The source is pulsed on for a period of time of t_p, the excitation pulse width (s). Phosphorescence is excited from the sample and decays exponentially following termination of the excitation pulse. After a suitable delay time, t_d(s), the signal from the detector is sampled for a fixed period of time, known as the aperature duration or gate width, t_g(s). The excitation/measurement cycle occurs at a repetition rate or frequency of f (Hz). The output signal level is proportional to the area under the emission decay curve bounded by the gate width. The exact nature of the relationship between signal level and area depends upon the specific measurement system employed. The theoretical advantages of the pulsed system over the conventional have been pointed out previously (7,8,14).

Figure 2. Schematic representation of the operation of a pulsed source gated phosphorimeter.

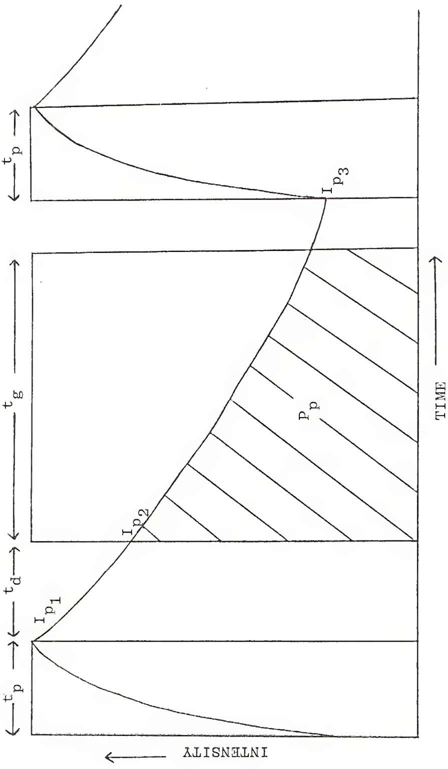
t_p
t_d
t_g
t_p
I_{p_1}
I_{p_2}
I_{p_3}
P_p
TIME
INTENSITY

These include increased precision resulting from increased signal-to-noise ratios (SNR), due to minimization of non-source-induced noise, and similar signal levels; lower detection limits resulting from increased SNR; and the ability to monitor phosphors having short lifetimes without interference from the slowly decaying trailing edge of a mechanically chopped excitation pulse. The most important advantage for application to TRP, however, is the versatility of the system, due to the relatively independent variability of the gate width, delay time, and repetition rate. It must be noted that in practical applications, the predicted increase in SNR has never been fully realized (26,27).

The recent trend in TRP instrumentation has been towards multichannel detection systems, such as the multichannel signal averager and the computer-controlled phosphorimeter, which monitor the entire emission decay curve following each excitation pulse (8-10,12,15). Sophisticated data handling techniques are also becoming common (15-18). However, there seems to be an enormous potential for applying less complex single channel instrumentation to TRP. This potential has never been adequately explored. The single channel or boxcar system can be used to monitor the entire emission decay curve by scanning the gate in time, but this is a time-consuming process. The strength of this type of system lies in measuring intensities at a few carefully selected times on the decay curve. Reasons for utilizing the pulsed source single channel gated detection system for TRP are as follows:

(i) Boxcar averager/integrators are "relatively" inexpensive and readily available;

(ii) The versatility of this type of instrument is enormous, due to the aforementioned independent adjustability of operating parameters;

(iii) Boxcar instruments are available to work on almost any time scale, from seconds to less than nanoseconds; this, coupled with the versatility, make possible a TRP analysis over a large range of sample lifetimes; some earlier systems were limited to either very rapidly decaying species (8) or very slowly decaying species (5), but not to both; and

(iv) The data manipulation can be as simple or as sophisticated as desired, while multichannel systems require manipulation of very large quantities of data, if the full potential of such an instrument is to be realized. This work is concerned with the application of a pulsed-laser source boxcar averager phosphorimeter to TRP. The advantages of the laser as a pulsed excitation source are well known, and include high peak powers, short pulse widths, variable repetition rate, and nearly monochromatic output.

It is important to realize that in most cases it is not possible to eliminate directly by time resolution the intensity contributions of all phosphors other than the one of interest; that is, one can not make a single intensity measurement and relate this to analyte concentration. What is usually necessary is to make intensity measurements at several times along the emission decay curve of the mixture, and then to extract mathematically (via simultaneous equations) the intensity contributions of the individual components. These deconvoluted intensities can then be related to the concentrations of the individual mixture components.

Fisher and Winefordner (8) described three methods for this type of data reduction, two of which are suitable for TRP using a single channel detection system. Both require that the individual phosphors comprising the sample mixture behave independently of one another, which must be true for all multicomponent phosphorimetric analyses. In the multiple-analytical-curve method (MAC), it is assumed that the analytical calibration curve (in linear coordinates) for a given phosphor has a slope which is dependent upon the delay time at which the intensity is measured (with f, t_p, and t_g constant). By setting up simultaneous equations stating that the total intensity at any one delay time is equal to the sum of the intensities of the individual components, expressions can be obtained which relate the concentrations of the individual phosphors to the intensity measurements obtained for the mixture. This method does not require knowledge of the lifetimes of the phosphors, but it is very time consuming, because it requires a calibration curve for each component at each delay time (n delay times required for an n-component mixture).

The exponential method (EM) is the technique chosen for this work. It does require measurement of the lifetimes of the individual components of the mixture, but these can be determined by scanning the single channel system. As mentioned earlier, this scanning process is relatively slow, but is required only for the initial determinations, and not for the actual intensity measurements on the mixture. The advantage of this method is that only one calibration curve is required per component, and thus the exponential method should be less time consuming overall than the MAC method, even when preliminary lifetime measurements are considered.

The working equations for EM are derived in the following manner (21). Let a hypothetical binary mixture consist of components A and B with lifetimes τ_A and τ_B, and let the intensities be measured at delay times t_{d_1} and t_{d_2}. Equation (2) can be rewritten specifically for the intensity contribution of A at delay time t_{d_1}

$$I_{A_1} = I_{A_0} \exp(-t_{d_1}/\tau_A) \tag{3}$$

where I_{A_0} is the initial intensity (at arbitrary or actual $t_d = 0$) of A. The equivalent expression for component B is

$$I_{B_1} = I_{B_0} \exp(-t_{d_1}/\tau_B) \tag{4}$$

Similar expressions can be written for the intensity contributions of A and B at delay time t_{d_2}. Because the total intensity, I_T, at any time is the sum of the intensities of A and B at that time,

$$I_{T_1} = I_{A_0} \exp(-t_{d_1}/\tau_A) + I_{B_0} \exp(-t_{d_1}/\tau_B) \tag{5}$$

and

$$I_{T_2} = I_{A_0} \exp(-t_{d_2}/\tau_A) + I_{B_0} \exp(-t_{d_2}/\tau_B) \qquad (6)$$

These two equations can be solved simultaneously for I_{A_0} and I_{B_0}, and these values, when substituted into Equations 3 and 4, yield I_{A_1} and I_{B_1}. Actually, once I_{A_0} and I_{B_0} are known, the intensities of A and B at any delay time, t_{d_N}, can be found by multiplying by $\exp(-t_{d_N}/\tau)$. The intensities so obtained can be used to determine the concentration of A and B from calibration curves prepared for pure solutions of A and B at delay time t_{d_N}. Fisher and Winefordner (8) and Fisher (21) derived the working equations for the two component mixture. These are presented in Table 1, in a form that will allow calculation of the intensity of that component at any delay time. The symbolism I_{X_N} refers to the intensity contribution of component X at delay time N. Note that the quantity in brackets is equal to the intensity of component X at $t_d = 0$ (I_{X_0}), and that this is multiplied by an exponential term to yield the intensity at various t_d's.

This same approach can be applied to a three component (ternary) mixture. In this case, there are three components, A, B, and C, with lifetimes τ_A, τ_B, and τ_C and three delay times, t_{d_1}, t_{d_2}, and t_{d_3}. Fisher calculated one of the expressions; the others were derived in this work. The three working equations are given in Table 2. It should be noted that, due to the complexity of the simultaneous equations, Cramer's Rule was required for their solution (28). Although the expressions appear formidable, if the exponential terms are calculated in advance, and inserted with the experimentally determined mixture intensities I_{T_1}, I_{T_2}, and I_{T_3}, the mathematics is easily handled on a pocket calculator.

An interesting question arises here. Only one calibration curve per component is required for the exponential method. However, the intensity contribution of any component can be calculated at any delay time. Under what conditions, then, should the single calibration curve be prepared? Certainly, the largest intensity would occur at $t_d = 0$ (although there are some practical limitations on using $t_d = 0$), and one would expect that preparing all calibration curves at the shortest delay time would yield optimum results. This minor point will be examined (experimentally) to some extent.

In order to insure that the results of such a multicomponent analysis have validity, there are several requirements that must be met. These were stated very clearly by Ridder and Margerum (16):

> multiple component analysis performed by the direct measurement of the physical properties of the components . . . must meet several general requirements. First, the number of measurements obtained at different values of the independent variable (i.e., wavelength, time, etc.) must be at least equal to the number of components to be determined (however, additional data may improve precision). Second, the relative contributions of the components at each measurement must not be redundant (i.e., there must be at least as many non degenerate equations

> as there are components). Third, the absolute and relative contributions of each component to the measurement must be large enough to achieve the sensitivity desired. . . . (p. 2098)

In TRP, the first requirement is met by taking measurements at as many different delay times as there are components to be quantitated. The second and third conditions for TRP may be explained as follows. Intensity measurements are made at different points in time, with the aim of correlating these mathematically to the experimental decays of the individual components. Obviously, each measurement must have significance (i.e., a good SNR). In addition, the delay times must be chosen in such a way as to insure a significant difference in total signal at the various points, because it is indirectly the difference in signal levels that contains the desired information. For experimental work, this requires that the difference in signal levels between the different times must be larger than the uncertainty of any of the measurements. Thus, it is necessary that the relative intensities of the mixture components differ significantly at the various delay times, and also that the total intensity varies significantly. Knowing in advance that the second and third conditions will be met is much more difficult, because it requires some prior knowledge of the relative intensities of the components, as well as the total intensities, at several sets of experimental conditions. Because the actual number of measurements required for a TRP analysis is large, and sampling in phosphorimetry is normally time consuming, it is obvious that trial and error selection of experimental conditions is not a viable choice, although this has been done (8).

Therefore, a large part of this work has explored how the choice of experimental conditions affects the relative intensity contributions from the individual components of a mixture, and how the conditions can be optimized for a particular separation.

The overall goal of this work is to examine the potential of a pulsed-laser source boxcar averager detection system for time resolved phosphorimetry. This is accomplished in part by deriving expressions relating observed phosphorescence intensity to the operating characteristics of the experimental system and to the lifetimes of sample components. This allows prediction of the relative effects of the various adjustable parameters, and gives insight into how the general requirements for multicomponent analysis can best be met for a given analysis. Experimental results are presented to verify the conclusions drawn from the theoretical work, which are then used to optimize the experimental system for TRP analysis of two-component and three-component mixtures of spectrally similar molecules.

TABLE 1
FINAL WORKING EQUATIONS FOR THE EXPONENTIAL METHOD OF TIME RESOLUTION FOR A BINARY MIXTURE

$$I_{A_N} = \left[\frac{I_{T_1}\exp(-t_{d_2}/\tau_B) - I_{T_2}\exp(-t_{d_1}/\tau_B)}{\exp(-t_{d_1}/\tau_A)\exp(-t_{d_2}/\tau_B) - \exp(-t_{d_1}/\tau_B)\exp(-t_{d_2}/\tau_A)}\right]\exp(-t_{d_N}/\tau_A) \qquad (7)$$

$$I_{B_N} = \left[\frac{I_{T_2}\exp(-t_{d_1}/\tau_A) - I_{T_1}\exp(-t_{d_2}/\tau_A)}{\exp(-t_{d_1}/\tau_A)\exp(-t_{d_2}/\tau_B) - \exp(-t_{d_1}/\tau_B)\exp(-t_{d_2}/\tau_A)}\right]\exp(-t_{d_N}/\tau_B) \qquad (8)$$

TABLE 2
FINAL WORKING EQUATIONS FOR THE EXPONENTIAL METHOD OF TIME RESOLUTION FOR A TERNARY MIXTURE

$$I_{A_N} = \left[\frac{(X)I_{T_1} + (Y)I_{T_2} + (Z)I_{T_3}}{(X)\exp(-t_{d_1}/\tau_A) + (Y)\exp(-t_{d_2}/\tau_A) + (Z)\exp(-t_{d_3}/\tau_A)}\right]\exp(-t_{d_N}/\tau_A) \qquad (9)$$

where

$$X = \exp(-t_{d_2}/\tau_B)\exp(-t_{d_3}/\tau_C) - \exp(-t_{d_2}/\tau_C)\exp(-t_{d_3}/\tau_B)$$

$$Y = \exp(-t_{d_1}/\tau_C)\exp(-t_{d_3}/\tau_B) - \exp(-t_{d_1}/\tau_B)\exp(-t_{d_3}/\tau_C)$$

$$Z = \exp(-t_{d_1}/\tau_B)\exp(-t_{d_2}/\tau_C) - \exp(-t_{d_1}/\tau_C)\exp(-t_{d_2}/\tau_B)$$

----

continued

TABLE 2-continued

$$I_{B_N} = \left[\frac{(X) I_{T_1} + (Y) I_{T_2} + (Z) I_{T_3}}{(X)\exp(-t_{d_1}/\tau_B) + (Y)\exp(-t_{d_2}/\tau_B) + (Z)\exp(-t_{d_3}/\tau_B)} \right] \exp(-t_{d_N}/\tau_B) \qquad (10)$$

where

$$X = \exp(-t_{d_2}/\tau_C)\exp(-t_{d_3}/\tau_A) - \exp(-t_{d_2}/\tau_A)\exp(-t_{d_3}/\tau_C)$$

$$Y = \exp(-t_{d_1}/\tau_A)\exp(-t_{d_3}/\tau_C) - \exp(-t_{d_1}/\tau_C)\exp(-t_{d_3}/\tau_A)$$

$$Z = \exp(-t_{d_1}/\tau_C)\exp(-t_{d_2}/\tau_A) - \exp(-t_{d_1}/\tau_A)\exp(-t_{d_2}/\tau_C)$$

---

continued

TABLE 2-continued

$$I_{C_N} = \left[\frac{(X)I_{T_1} + (Y)I_{T_2} + (Z)I_{T_3}}{(X)\exp(-t_{d_1}/\tau_C) + (Y)\exp(-t_{d_2}/\tau_C) + (Z)\exp(-t_{d_3}/\tau_C)}\right]\exp(-t_{d_N}/\tau_C) \qquad (11)$$

where

$$X = \exp(-t_{d_2}/\tau_A)\exp(-t_{d_3}/\tau_B) - \exp(-t_{d_2}/\tau_B)\exp(-t_{d_3}/\tau_A)$$

$$Y = \exp(-t_{d_1}/\tau_B)\exp(-t_{d_3}/\tau_A) - \exp(-t_{d_1}/\tau_A)\exp(-t_{d_3}/\tau_B)$$

$$Z = \exp(-t_{d_1}/\tau_A)\exp(-t_{d_2}/\tau_B) - \exp(-t_{d_1}/\tau_B)\exp(-t_{d_2}/\tau_A)$$

CHAPTER II
THEORETICAL CONSIDERATIONS

In this chapter, the theoretical aspects of TRP will be dealt with. First, the kinetic events occurring during excitation and initiation of phosphorescence emission will be discussed. The results of this analysis, coupled with the knowledge of how the gated detection system responds to the emitted luminescence, yields an expression which relates measured signal level to the parameters of excitation pulse width, repetition rate, delay time, gate width, and phosphorescence lifetime, τ, of the analyte. This expression is used as a basis for predicting the effects of the individual parameters, and how these parameters may be optimized for a particular phosphorimetric analysis.

Kinetic Analysis of Molecular Processes (29)

This section is a summary of the conclusions reached by McGlynn, Srinivasan, and Maria (29) in a superb paper on the kinetic processes occurring during phosphorescence. The details of the mathematical model and the derivations employed are presented in the Appendix. Tables and figures are reprinted by permission of the publisher.

The system studied is a phosphor species frozen into a glassy matrix. This matrix gives good optical characteristics, and minimizes solute-solute interactions. In this matrix, decay is usually first order (exponential), and the concept of mean phosphorescence lifetime is valid. As stated earlier in this work, τ refers to the experimentally observed phosphorescence decay lifetime. The analysis in the Appendix approximates τ as a function of fundamental rate constants for the processes involved in excitation/de-excitation of the triplet state. There is, however, another lifetime associated with a phosphor, this being the phosphorescence growth lifetime, designated τ^R (R for rise). The growth lifetime describes the rate of phosphorescence intensity increase when a phosphor sample is irradiated. What is predicted theoretically, and observed experimentally, is that the observed phosphor intensity grows exponentially while the excitation continues, eventually reaching a steady state value. This steady state intensity level is designated I_0 and is the maximum intensity observable for that sample and experimental system.

The actual relationship describing the growth of phosphorescence when the sample is subjected to constant intensity irradiation is

$$I = [1-\exp(-t/\tau^R)]I_0 \qquad (12)$$

where I is the intensity at time t. In addition to Equation 12, the difference between τ and τ^R is of great interest. It has been found that in many cases, τ and τ^R

are not identical, but that $\tau^R \lesssim \tau$. The magnitude of the difference between the two is expected to increase when τ is large, when the quantum efficiency for intersystem crossing is large, and when the excitation intensity is large. In the limit of very small excitation intensity, the difference between τ and τ^R approaches zero. Experimental comparisons of the growth and decay of a number of phosphors were cited, and the results included values for naphthalene, with $\tau^R = 16.6$ s and $\tau = 19.9$ s; for triphenylene, with $\tau^R = 10.4$ s and $\tau = 13.4$ s; and for phenanthrene, with $\tau^R = 3.3$ s, and $\tau = 3.9$ s. The difference between τ^R and τ varies from 8% to 25% for these phosphors.

Intensity Expressions

O'Haver and Winefordner (3,4) derived an expression which related the observed phosphorescence intensity to the temporal characteristics of the luminescence and to the operating parameters of the measurement system. The system discussed was an averaging DC meter. The resulting expression contained observed luminescence intensity dependence upon τ, t_p, f, t_d, and t_g. Plots of relative intensity versus lifetime (other parameters constant) showed distinctive features, the most significant of which was that under various combinations of experimental parameters, there was a point of maximum intensity, corresponding to a particular phosphorescence lifetime. The lifetime corresponding to the point of maximum instrumental response is designated τ_{max}. By using simplifying assumptions, it was possible to derive an expression that enabled one to choose the experimental conditions to shift that point of maximum response to a given phosphor lifetime. Possible applications were given, such as calculating theoretical analyte/interferent intensity ratios based on their lifetimes. No experimental evidence for validation of the underlying model was given. In addition, the expression allowing calculation of optimum experimental conditions was based on an assumption which invalidates the expression for some very useful practical cases.

In this chapter, a similar expression will be derived. There will be several major differences,however. The measurement system employed for this derivation is the gated (boxcar) averager. In the initial derivation, a distinction is made between phosphorescence growth lifetime, τ^R, and phosphorescence decay lifetime, τ. Later, the expression for optimization will be derived in such a way as to be valid over a much wider range of conditions. Most importantly, major emphasis will be placed upon trying to explain on a physical basis the trends predicted from this theoretical analysis. The underlying factor throughout this chapter is the search for results of practical applicability.

The concept of exponential growth of phosphorescence during irradiation is critical to the following derivations.

Although the previous section states the reality of this growth process, it is somehow difficult at first inspection to rationalize the premise of a long lifetime for phosphorescence growth. It seems to contradict what is known about the rapid population of the triplet state by intersystem crossing following the absorption of photons.

The fallacy is, of course, that although the excitation process for one molecule is very fast, what is observed experimentally is the luminescence emitted from a very large number of excited molecules. One could simplistically visualize an excitation pulse beginning at time $t = 0$ and continuing indefinitely. Let the excitation be temporally subdivided into a very large number of small segments of excitation intensity. By assuming only that the excitation process is very rapid, the following rationalization emerges. During the first excitation segment, a number of molecules, n, undergo absorption and subsequent population of the triplet state. Species in the triplet state will undergo deactivation via the characteristic exponential phosphorescence decay, $\exp(-t/\tau)$. During each subsequent excitation segment, a population of n molecules are excited and phosphorescence. Although the excitation process for any subset of n molecules is very rapid, what is actually observed is the sum of phosphorescence intensity decays from a very large number of subsets of excited molecules. It can be seen that the overall phosphorescence intensity will continue to increase until the intensity contributed by the very first subset of excited molecules disappears. After this occurs, i.e., all of the molecules excited during the first excitation segment have returned to the ground state, the observed phosphorescence intensity will reach a steady state, because equal numbers of molecules are excited and deactivated at each instant. This steady state intensity is the I_0 described earlier and will not be exceeded, regardless of how much longer the sample is irradiated. I_0 represents the phosphorescence intensity level resulting from continuous (CW) excitation. Almost five phosphorescence decay lifetimes are required for phosphorescence intensity to decay to 1% of its initial value. Thus, it could take only milliseconds of excitation for a short-lived phosphor to reach I_0, but a long-lived phosphor might require ten seconds or longer. If the excitation is terminated (as with a pulsed source) before a sufficient time period has elapsed, the observed phosphorescence intensity will be some fraction of I_0.

This same reasoning can be used to describe the excitation process in a pulsed system. Figure 3 illustrates a train of excitation pulses of width t_p occurring at the rate of f pulses per second. During each excitation pulse, the phosphorescence grows proportionately to τ^R, and the

Figure 3. Schematic representation of the excitation process with a pulsed source.

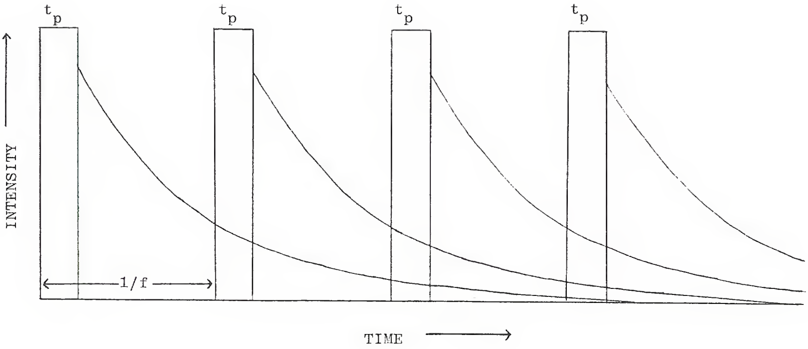
t_p
t_p
t_p
t_p
INTENSITY
1/f
TIME

intensity at the end of the first pulse is given by $I_0[1-\exp(-t_p/\tau^R)]$. When this pulse ends, the phosphorescence intensity decays. This takes place independently on each successive excitation pulse, with each pulse contributing the same amount of additional phosphorescence intensity. The observed intensity is the sum of the intensities resulting from all the preceding pulses. Therefore, one would expect that if a train of excitation pulses is incident upon a non excited "phosphorescent" sample, the phosphorescence intensity would rise rapidly during each pulse, and would decay between pulses. Also, that the intensity immediately following the pulse would increase steadily, as "new" intensity (that due to the latest pulse) is added to the intensity still present from the previous pulses. Again, after some number of pulses, the pulse-to-pulse intensity would reach some "pulsed source steady state," with the additional intensity from any pulse balancing the loss of intensity due to decay. The time required to reach this steady state should be independent of repetition rate, but should depend on the decay lifetime, τ, of the phosphor. It is not improper, then, to speak of "pulse-to-pulse phosphorescence intensity growth," when the intensity is observed at the same time relative to each pulse.

The operation of the pulsed source gated detection system of Figure 2 can now be examined further. The intensity and time axes are not to scale. The excitation pulse, of width t_p, is an extremely short, high intensity burst of radiation, which is assumed to have the shape of a step function. That is, it goes instantaneously from zero intensity to maximum intensity, and maintains this level for t_p seconds. The phosphorescence intensity grows during t_p and decays between pulses as previously discussed. If the excitation pulse had sufficient duration, the intensity would reach I_0. For this derivation, it is assumed that a sufficiently large number of pulses have been incident on the sample, that the "pulse-to-pulse steady state" has been attained. This means that in Figure 2, the loss of intensity due to decay from I_{P_1} to I_{P_3} is equal to the increase in intensity from I_{P_3} to I_{P_1}. For convenient reference, important variables are listed in Table 3.

I_{P_3} is the instantaneous intensity at the start of any excitation pulse, and includes the intensity resulting from many previous excitation pulses. During the pulse, the intensity level will continue to decay, and at the end of t_p, the remaining intensity will be

$$I_{P_3} \exp(-t_p/\tau) \qquad (13)$$

TABLE 3
DEFINITION OF PARAMETERS

Symbol	Definition
t_p	excitation pulse width, s
t_d	delay time, s
t_g	gate width, s
I_0	CW phosphorescence intensity
I/I_0	Relative phosphorescence intensity, unitless
τ	Phosphorescence decay lifetime, s
τ^R	Phosphorescence growth lifetime, s
I_p	Instantaneous phosphorescence intensity
I_{p_1}	I_p immediately following t_p
I_{p_2}	I_p at the leading edge of t_g
I_{p_3}	I_p at the leading edge of t_p
P_p	Integrated luminescence intensity observed (per excitation/emission cycle)

However, during t_p, intensity growth occurs, and the intensity added per pulse is given by Equation 12,

$$I = I_0[1-\exp(-t_p/\tau^R)]$$

Therefore, the instantaneous intensity immediately following t_p is the sum of these two contributions,

$$I_{P_1} = I_{P_3}\exp(-t_p/\tau)+I_0[1-\exp(-t_p/\tau^R)] \qquad (14)$$

However, I_{P_3} is simply I_{P_1} after decay for a period of time equal to the total time per cycle, 1/f, minus the pulse width, t_p:

$$I_{P_3} = I_{P_1}\exp[-(1/f-t_p)/\tau] \qquad (15)$$

Substituting for I_{P_3} in Equation 14,

$$I_{P_1} = I_{P_1}\exp[-(1/f-t_p)/\tau]\exp(-t_p/\tau)+I_0[1-\exp(-t_p/\tau^R)] \quad (16)$$

By combining exponentials and solving, one finds

$$I_{P_1} = \frac{I_0[1-\exp(-t_p/\tau^R)]}{[1-\exp(-1/f\ \tau)]} \qquad (17)$$

I_{P_1} is the maximum instantaneous phosphorescence obtained per cycle. However, the instantaneous intensity present at the leading edge of the gate, I_{P_2}, is less than I_{P_1}, due to decay over a period of time equal to t_d. Thus,

$$I_{P_2} = I_{P_1}\exp(-t_d/\tau) \qquad (18)$$

and substituting into Equation 17 for I_{P_1} yields

$$I_{P_2} = \frac{I_0[1-\exp(-t_p/\tau^R)]\exp(-t_d/\tau)}{[1-\exp(-1/f\ \tau)]} \qquad (19)$$

At any time during the gate, the instantaneous intensity is given by

$$I_P = I_{P_2}\ \exp(-t/\tau) \qquad (20)$$

The observed integrated phosphorescence intensity per cycle, P_p (the shaded area in Figure 2), is the integral of the intensity during the gate width:

$$P_p = \int_0^{t_g} I_P dt = \int_0^{t_g} I_{P_2} \exp(-t/\tau)dt \qquad (21)$$

$$P_p = I_{P_2} \int_0^{t_g} \exp(-t/\tau)dt \qquad (22)$$

$$P_p = I_{P_2}\ \tau[1-\exp(-t_g/\tau)] \qquad (23)$$

Substituting for I_{P_2} from Equation 19 yields

$$P_p = \frac{I_0\ \tau[1-\exp(-t_g/\tau)][1-\exp(-t_p/\tau^R)]\exp(-t_d/\tau)}{[1-\exp(-1/f\ \tau)]} \qquad (24)$$

The boxcar or gated averager measures signal levels by averaging the intensity over each gate, and then averaging the average intensity per gate over many gates (30,31). Thus, for the boxcar averager the signal level is proportional to P_p/t_g. Therefore, for the pulsed source gated averager system,

$$I= \frac{I_0 \ \tau[1-\exp(-t_p/\tau^R)][1-\exp(-t_g/\tau)]\exp(-t_d/\tau)}{t_g[1-\exp(-1/f \ \tau)]} \qquad (25)$$

Equation 25 is the basis from which all remaining expressions will be derived. Thus far, no assumptions have been made regarding the relative magnitudes of the various parameters, and Equation 25 is quite general. Note that Equation 24 for P_p, can also be validly applied to the boxcar or gated integrator. The integrator sums the integrated observed phosphorescence intensity per cycle, and

$$I = P_p \ f \ t_c \qquad (26)$$

where t_c is the counting time. The signal level is simply equal to the area per gate times the number of gates summed. For the averaging DC meter (4),

$$I = f \ P_p \qquad (27)$$

At this point, several assumptions will be made to simplify Equation 25 and to put it in a form more conducive to practical application. The first assumption is that the phosphorescence growth lifetime, τ^R , is approximately equal to the phosphorescence decay lifetime, τ. This is done for several reasons. First, in the majority of cases, the error introduced by this assumption should be negligible. The difference between τ and τ^R could easily lie within the standard deviation of the normal lifetime determination in many cases. Also, the thrust of this work is to study primarily the relative dependencies of intensity upon experimental parameters, and an absolute relationship is not essential. Finally, a relationship containing only τ would be more easily applied than if both lifetimes were required. Phosphorescence decay lifetimes are readily available in the literature for many compounds, and are easily measured with standard phosphoroscopic instrumentation, while growth lifetimes are seldom quoted and require modification of the phosphorimeter for measurement.

It is certainly important to realize that τ and τ^R may differ, and under what conditions this difference is maximized. As the difference between τ and τ^R increases, the expressions may begin to show error. This is the reason for including the kinetic summary in the preceding section.

The second assumption is easily met by most pulsed source phosphorimeters. We assume that the excitation pulse width, t_p, is much smaller than the sample lifetime, $t_p << \tau$. Thus, the excitation pulse is limited to 10^{-4}s for the shortest lived phosphors ($\tau \sim$1ms). Most pulsed sources have pulse widths of microseconds or less, and so this assumption should be valid. If the case should arise where $\tau \approx t_p$, Equation (25) would be necessary. With the assumptions $\tau^R = \tau$ and $t_p << \tau$, the growth term $[1-\exp(-t_p/\tau^R)]$ can be expanded and approximated by t_p/τ.

Therefore, Equation 25 reduces to

$$I = I_0 \frac{t_p}{t_g} \frac{[1-\exp(-t_g/\tau)]\exp(-t_d/\tau)}{[1-\exp(-1/f\ \tau)]} \qquad (28)$$

It should be possible to derive a similar expression by relying upon the additivity of intensity from pulse to pulse. Each excitation pulse yields phosphorescence intensity as given by Equation 12. Let this intensity growth per pulse be designated I_G. Let the last pulse be designated as pulse "N," and preceding pulses as "N-1," "N-2," etc. At the termination of pulse N, the intensity decays resulting from preceding pulses have decayed for various periods of time, given by some number of 1/f (s) periods. Intensity resulting from pulse N has decayed for zero cycles, pulse N-1 for 1 cycle, and so on. Therefore, after N pulses, the total intensity, I_T, could be given by

$$I_T=I_G+I_G[\exp(-1/f\ \tau)]+I_G[\exp(-2/f\ \tau)]+\ldots+I_G[\exp(-N/f\,\tau)] \qquad (29)$$

or

$$I_T = I_G \sum_{i=0}^{N} e^{-i/f\,\tau} \qquad (30)$$

If N is large,

$$I_T = I_G \int_0^{\infty} e^{-i/f\,\tau}\ di \qquad (31)$$

But

$$\int e^{ax}\, dx = e^{ax}/a \qquad (32)$$

so, if $a = -1/f\ \tau$,

$$I_T = I_G \, [e^{-i/f\,\tau} \, (-f\,\tau)]_0^{\infty} \qquad (33)$$

Substitution and evaluating yields

$$I_T = I_G \, f \, \tau \qquad (34)$$

Since I_T is the intensity following t_p at steady state (N large), $I_T = I_{P_1}$ in Figure 2, and since I_G is defined by Equation 12,

$$I_{P_1} = f \, \tau \, I_0 [1\text{-}\exp(-t_p/\tau^R)] \qquad (35)$$

The remainder of the derivation would then follow that already presented in Equations 17-28. Comparing Equations 35 and 17 shows that they are not identical; however, in the limit of small $1/f\,\tau$ (large f or large τ), the two converge. Why this difference occurs is not clear. However, the similarity of the results for the limiting case indicates that there is validity in the underlying principle of the second derivation.

Applications

From a practical point of view, Equation 28 is very important, for it allows one to ascertain the relative effects of t_p , t_g , t_d , f , and τ on the observed intensity. Note that the observed intensity, I , is some fraction of I_0 . Dividing I by I_0 would essentially normalize to a constant CW intensity level,

$$I/I_0 = \frac{t_p}{t_g} \; \frac{[1\text{-}\exp(-t_g/\tau)]\exp(-t_d/\tau)}{[1\text{-}\exp(-1/f\,\tau)]} \qquad (36)$$

I/I_0 can be termed the "relative response" of the detection system, and is actually the effective duty factor for the measurement (26,30). A plot of I/I_0 versus τ with t_p , t_g , t_d , and f fixed gives a plot of the relative response of the instrumentation as a function of sample lifetime. The terms "relative response" and "relative intensity" will be used interchangeably.

A typical "relative response profile" resembles Figure 4. The most significant feature is that there is a lifetime corresponding to an optimum response, designated τ_{max}. Relative intensity falls off rapidly towards longer (τ_L) and shorter (τ_S) lifetimes. The "enhancement ratios," or ratios of relative intensity values, for τ_{max} over τ_S and τ_L can be approximated by reading off the intensities I_{max} , I_S , and I_L , and calculating I_{max}/I_S and I_{max}/I_L . There is a lower boundary on relative intensity at long τ. This occurs when $\tau >> 1/f$, t_p , t_d , and t_g . Under these conditions, $[1-\exp(-t_g/\tau)]$ is approximately equal to t_g/τ , $\exp(-t_d/\tau)$ approaches unity, and $[1-\exp(-1/f\ \tau)]$ is approximately equal to $1/f\ \tau$. Therefore, Equation 28 reduces to

$$I/I_0 = t_p\ f \qquad (37)$$

The gated detection system has enhanced response to τ_{max} , and discriminates against other lifetime components, both longer and shorter. The time resolution system is, in effect, a "time filter," and the relative response profile could be compared to the wavelength response profile

Figure 4. A typical relative response profile.

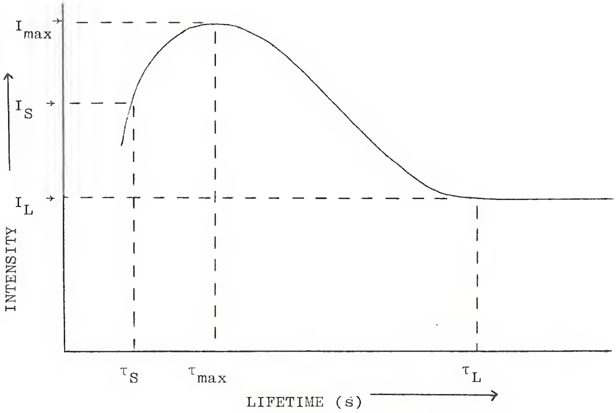
I_{max}
I_S
I_L
INTENSITY
τ_S
τ_{max}
τ_L
LIFETIME (s)

of an optical filter, or the frequency response profile of an electrical filter.

It would be very useful to be able to alter the shape of the response profile, and to change τ_{max} as desired. This would make it much easier to tailor the experimental system for a particular analysis. A way to attack this is to take the derivative of I/I_0 with respect to τ , and set the derivative equal to zero.

Optimization Expression for t_d

From Equation 28,

$$(I/I_0)(t_g/t_p) = \frac{\exp\ (-t_d/\tau)[1-\exp(-t_g/\tau)]}{[1-\exp(-1/f\ \tau)]} \qquad (38)$$

Taking the derivative with respect to τ and setting it equal to zero,

$$dI/d\tau = 0 = d_\tau \left[\frac{\exp\ (-t_d/\tau)[1-\exp(-t_g/\tau)]}{[1-\exp(-1/f\ \tau)]}\right] \qquad (39)$$

By using standard calculus techniques (28), we obtain

$$[\exp(-t_d/\tau)(t_d/\tau^2)-(\exp[-(t_d+t_g)/\tau])(t_d+t_g)/\tau^2\ ] \times$$
$$[1-\exp(-1/f\ \tau)]=[-\exp(-1/f\ \tau)](1/f\ \tau^2)([\exp(-t_d/\tau)]-$$
$$\exp[-(t_d+t_p)/\tau]) \qquad (40)$$

Factoring yields

$$[1-\exp(-1/f\ \tau)][\exp(-t_d/\tau)][(t_d/\tau^2)-\exp(-t_g/\tau)(t_d+t_g)/\tau^2\ ]=$$
$$[-\exp(-1/f\ \tau)](1/f\ \tau^2)[\exp(-t_d/\tau][1-\exp(-t_g/\tau)] \quad (41)$$

Further simplification is algebraic, and the necessary manipulations are:

(1) division by $\exp(-t_d/\tau)$

(2) multiplication by τ^2

(3) division by $[1-\exp(-1/f\ \tau)]$

(4) expansion of the first term

(5) addition of $t_g \exp(-t_g/\tau)$ to both sides; and

(6) division by $[1-\exp(-t_g/\tau)]$

These steps yield

$$t_d = \frac{(-1/f)[\exp(-1/f\ \tau)]}{[1-\exp(-1/f\ \tau)]} + t_g \frac{[\exp(-t_g/\tau)]}{[1-\exp(-t_g/\tau)]} \qquad (42)$$

By dividing out each term, the final result is obtained:

$$(t_d)_{opt} = t_g \left[\frac{1}{\exp(t_g/\tau)-1}\right] - (1/f)\left[\frac{1}{\exp(1/f\ \tau)-1}\right] \qquad (43)$$

This expression calculates the optimum delay time, $(t_d)_{opt}$, required to optimize the response of the instrumentation to any given lifetime, τ, at fixed t_g and f. There is no dependence upon t_p, due to the earlier assumption regarding t_p. Equation 43 is also valid for the gated integrator system, since the conversion factor is multiplicative, and disappears when the derivative is set equal to zero.

O'Haver and Winefordner (4) give a similar expression for the DC averaging meter system, but with the assumption that $t_p \ll \tau \ll 1/f$. Their expression is

$$(t_d)_{opt} = t_g \left[\frac{1}{\exp(t_g/\tau)-1}\right] \qquad (44)$$

If the limitation $\tau \ll 1/f$ is applied to Equation 43,

$1/f\,\tau$ grows large, $\exp(1/f\,\tau)$ approaches infinity, and the frequency dependent term drops out. Thus, within the limits of Equation 44, the two expressions are identical.

Equation 43 is also of practical importance, because it allows rapid evaluation of instrumental parameters for a sample of given lifetime. For further study and convenience of application, plots of $(t_d)_{opt}$ versus τ at constant f and t_g were prepared. The plots were obtained by programming Equation 43 into a Hewlett-Packard 25 calculator, and evaluating the various terms. The results were plotted on oversize sheets of log-log graph paper, and were later photographically reduced.

The sets of parameters were chosen to be representative of the operating characteristics of practical experimental systems, and specifically those of the source/detection system used later in this work. Repetition rates of 1, 10, and 50 Hz were chosen, and a wide range of gate widths was used. The plots are keyed to the various gate widths as shown in Table 4. One microsecond was taken as the lower limit on gate width. The results are shown in Figures 5-7. Each figure gives the curves corresponding to the various gate widths at constant repetition rate.

Examination shows several interesting features. Distinct regions can be observed for each curve, roughly corresponding to long, intermediate, or short lifetimes.

TABLE 4
KEY TO GATE WIDTH FOR FIGURES 5-7

Gate width (t_g), s	Legend
$1x10^{-5}$	A
$5x10^{-5}$	B
$1x10^{-4}$	C
$5x10^{-4}$	D
$1x10^{-3}$	E
$5x10^{-3}$	F
$1x10^{-2}$	G
$5x10^{-2}$	H
$9x10^{-2}$	I

Figure 5. Optimum delay versus lifetime (f = 1 Hz).

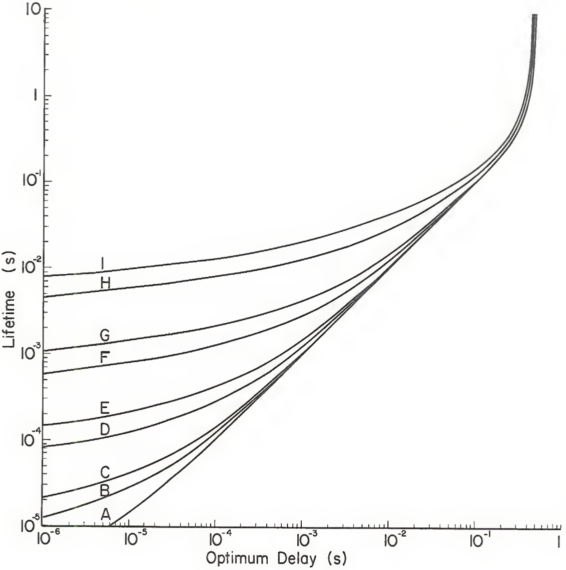
Lifetime (s)
10
1
10⁻¹
10⁻²
10⁻³
10⁻⁴
10⁻⁵
I
H
G
F
E
D
C
B
A
10⁻⁶
10⁻⁵
10⁻⁴
10⁻³
10⁻²
10⁻¹
1
Optimum Delay (s)

Figure 6. Optimum delay versus lifetime (f = 10 Hz).

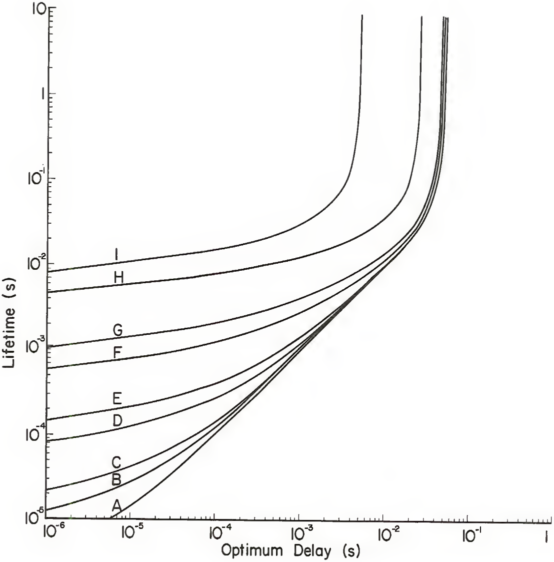
Lifetime (s)
10
1
10^{-1}
10^{-2}
10^{-3}
10^{-4}
10^{-5}
I
H
G
F
E
D
C
B
A
10^{-6}
10^{-5}
10^{-4}
10^{-3}
10^{-2}
10^{-1}
1
Optimum Delay (s)

Figure 7. Optimum delay versus lifetime (f = 50 Hz).

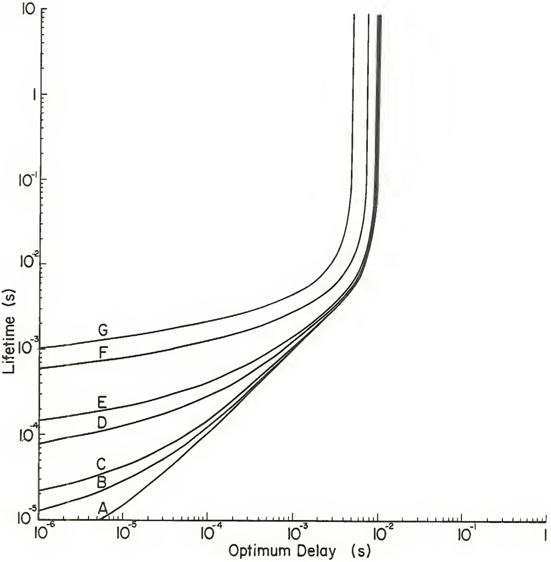
Lifetime (s)
10
1
10^{-1}
10^{-2}
10^{-3}
10^{-4}
10^{-5}
Optimum Delay (s)
10^{-6}
10^{-5}
10^{-4}
10^{-3}
10^{-2}
10^{-1}
1
G
F
E
D
C
B
A

In the 50 Hz plot, Figure 7, gate widths H and I do not appear. This is due to the physical boundary conditions of the real system. The total time between successive excitation pulses is 1/f (s). This must be larger than the sum of the pulse width, delay time, and gate width. At 50 Hz, 1/f = 0.02 s, and therefore no gate widths larger than this are possible.

At the long lifetime limit, the optimum delay is asymptotic, and shows little change with lifetime. The asymptote is gate width dependent, and shifts the optimum delay to smaller values at higher frequencies. The implication of this asymptotic behavior is that at long lifetimes, since $(t_d)_{opt}$ is independent of lifetime, the gated detection system will not be able to discriminate between phosphors with lifetimes in this region.

Mathematically, the reason for this behavior can be explained. By expanding the exponential terms in Equation 43 and retaining first and second order terms, we obtain

$$(\frac{1}{f})\left[\frac{1}{\exp(1/f\ \tau)-1}\right] = \frac{1}{f}\left[\frac{1}{\frac{1}{f\tau} + \frac{1}{2(f\ \tau)^2}}\right] = \frac{\tau}{1+\ \frac{1}{2f\ \tau}} \qquad (45)$$

and

$$t_g\ \left[\frac{1}{\exp(t_g/\tau)-1}\right] = t_g\ \left[\frac{1}{t_g/\tau + \frac{1}{2}(t_g/\tau)^2}\right] = \frac{\tau}{1 + t_g/2\tau} \qquad (46)$$

Therefore,

$$(t_d)_{opt} = \frac{\tau}{1 + t_g/2\tau} - \frac{\tau}{1 + 1/2f\ \tau} \qquad (47)$$

Finding the common denominator and combining terms gives

$$(t_d)_{opt} = 2\tau^2 \left[\frac{1/f - t_g}{(2\tau + t_g)(2\tau + 1/f)}\right] \qquad (48)$$

if the assumption is made that $2\tau >> t_g$, $1/f$,

$$(t_d)_{opt} = 2\tau^2 \left[\frac{1/f - t_g}{4\tau^2}\right] = \frac{1/f - t_g}{2} \qquad (49)$$

Thus, for very long lifetimes (relative to t_g and $1/f$), $(t_d)_{opt}$ is constant, and is exactly one-half of the maximum possible delay, $1/f - t_g$ (t_p negligible). Equation 49 does predict correctly the asymptote in Figure 5-7.

In the limit of shorter lifetimes (left-hand section), the curves are frequency independent. This is expected, because in this region, Equation 44 is valid. In the central region of the Figures, the curves for longer gate widths exhibit curvature. However, as the gatewidths decrease, the curves approach linearity, with $(t_d)_{opt} = \tau$. This can be shown to occur when $t_g < \tau$ and $\tau < 1/f$.

Because the left-hand boundary of the figures represents the smallest delay time attainable on a practical level, the lifetime corresponding to $(t_d)_{opt} = 10^{-6}$ s is the smallest lifetime that can be realistically optimized at that f and t_g. As t_g decreases (curves I to A), the $(t_d)_{opt}$ for smaller lifetimes becomes accessible.

There is another physical constraint of great significance. As noted earlier, the boxcar averager averages the signal over a large number of gate widths. If enough gates are averaged, random fluctuations (noise) in the signal should cancel, and the output should approach the average signal level of P_p/t_g. This signal-to-noise ratio (SNR) enhancement is accomplished by using an RC filter. Most measurement instruments possess a time constant, which indicates how rapidly the instrument can respond to an applied signal. The normal measurement procedure is to actually measure the signal for a period of time equal to five time constants, to insure adequate time for the instrument to respond. In the gated system, the signal is only sampled during the gate width, which is a small fraction of the total measurement time. The fraction, actual measurement time divided by total measurement time, is known as the duty factor, $D_f = f \times t_g$. The RC filter in the system necessitates that the signal be actually applied to the filter section for 5 x RC. Because the signal is actually sampled only a fraction, D_f, of the total time, with the boxcar averager the total measurement time required is

$$5\left[\frac{RC}{f\ t_g}\right]$$

where the quantity in brackets is known as the observed time constant, OTC. Thus, the actual measurement time for the boxcar averager is five times OTC.

Since the value of RC selected effectively determines the SNR of the measurement, if the noise is not directly related to f or t_g, the measurement time required to obtain the same SNR decreases as f or t_g increases. Conversely, as f or t_g is decreased, the OTC, and thus the actual measurement time, increases proportionately.

Response Profiles

If t_p, t_g, and f are known, $(t_d)_{opt}$ can be calculated, which will give maximum enhancement to intensity at the lifetime, τ, chosen. The parameters thus selected can be used in conjunction with Equation 28 to calculate response profiles with maxima at selected lifetimes, under various experimental conditions. Such profiles will be presented here, and are used to ascertain the effects of f, t_d and t_p on the observed intensity levels.

The plots are prepared in a similar fashion to those shown previously. The values of the parameters represent realistic experimental conditions. It was necessary to limit the number of values studied per parameter, but those values selected for each factor cover a fairly broad range. Four repetition rates (f = 1, 10, 50, 100 Hz) and three gate widths ($5x10^{-3}$, $5x10^{-4}$, $5x10^{-5}$s) are employed. The excitation pulse width, t_p, is 10^{-8}s, and is representative of the nitrogen laser pulse used later in this study.

For each combination of frequency and gate width, $(t_d)_{opt}$'s are calculated to yield a family of response profiles, with maximum response occurring at lifetimes of 9, 0.9, $9x10^{-2}$, $9x10^{-3}$, $9x10^{-4}$, and $9x10^{-5}$s. The optimum delays calculated for the various combinations of f, t_g, and τ are given in Table 5, which also contains the legend used to identify the curves. Every curve marked "A" should have maximum response at $\tau = 9$ s, curves marked "B" at 0.9s, and so on. In addition, a curve marked "G" appears on one figure. For this curve, the delay time used was the maximum physically attainable delay, $1/f - t_g$ (remember the asymptote at long τ is equal to 1/2 of this quantity). This was included to demonstrate that delays other than the $(t_d)_{opt}$ predicted at long lifetimes can be used.

The resulting families of response profiles of relative intensity versus lifetime are presented in Figures 8-19. Each figure represents a fixed frequency and gate width, with the individual curves varying only in delay time. Any one curve represents the relative response of the experimental system under one fixed set of experimental conditions.

TABLE 5
PARAMETERS FOR RESPONSE PROFILES

τ_{max}(s) =			9	9×10^{-1}	9×10^{-2}	9×10^{-3}	9×10^{-4}	9×10^{-5}
Legend:			A	B	C	D	E	F
Fig.	t_g(s)	f(Hz)	Optimum Delays (s)					
8	5×10^{-3}	1	4.88×10^{-1}	4.07×10^{-1}	8.75×10^{-2}	6.73×10^{-3}	1.94×10^{-5}	-
9	5×10^{-3}	10	4.74×10^{-2}	4.66×10^{-2}	3.84×10^{-2}	6.73×10^{-3}	1.94×10^{-5}	-
10	5×10^{-3}	50	7.50×10^{-3}	7.47×10^{-3}	7.15×10^{-3}	4.30×10^{-3}	1.94×10^{-5}	-
11	5×10^{-3}	100	2.50×10^{-3}	2.49×10^{-3}	2.43×10^{-3}	1.82×10^{-3}	1.93×10^{-5}	-
12	5×10^{-4}	1	4.91×10^{-1}	4.09×10^{-1}	8.97×10^{-2}	8.75×10^{-3}	6.73×10^{-4}	1.94×10^{-6}
13	5×10^{-4}	10	4.97×10^{-2}	4.88×10^{-2}	4.07×10^{-2}	8.75×10^{-3}	6.73×10^{-4}	1.94×10^{-6}
14	5×10^{-4}	50	9.75×10^{-3}	9.71×10^{-3}	9.38×10^{-3}	6.32×10^{-3}	6.73×10^{-4}	1.94×10^{-6}
15	5×10^{-4}	100	4.77×10^{-3}	4.74×10^{-3}	4.66×10^{-3}	3.84×10^{-3}	6.73×10^{-4}	1.94×10^{-6}
16	5×10^{-5}	1	4.90×10^{-1}	4.09×10^{-1}	9.00×10^{-2}	8.98×10^{-3}	8.75×10^{-4}	6.73×10^{-5}
17	5×10^{-5}	10	4.92×10^{-2}	4.91×10^{-2}	4.09×10^{-2}	8.97×10^{-3}	8.75×10^{-4}	6.73×10^{-5}
18	5×10^{-5}	50	9.98×10^{-3}	9.94×10^{-3}	9.60×10^{-3}	6.54×10^{-3}	8.75×10^{-4}	6.73×10^{-5}
19	5×10^{-5}	100	4.98×10^{-3}	4.97×10^{-3}	4.88×10^{-3}	4.07×10^{-3}	8.75×10^{-4}	6.73×10^{-5}

Figure 8. Response profile ($t_g = 5 \times 10^{-3}$ s, f = 1 Hz).

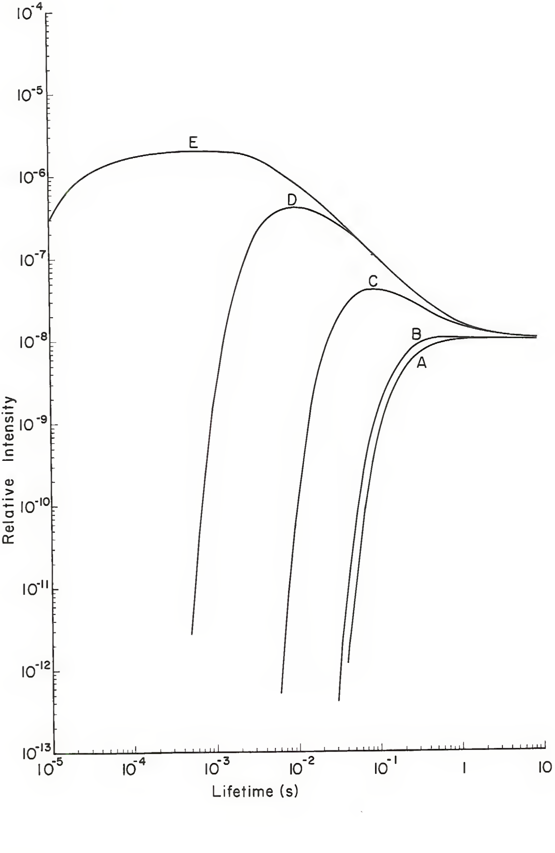

10^{-4}
10^{-5}
10^{-6}
10^{-7}
10^{-8}
10^{-9}
10^{-10}
10^{-11}
10^{-12}
10^{-13}
Relative Intensity
E
D
C
B
A
10^{-5}
10^{-4}
10^{-3}
10^{-2}
10^{-1}
1
10
Lifetime (s)

Figure 9. Response profile ($t_g = 5x10^{-3}s$, $f = 10$ Hz).

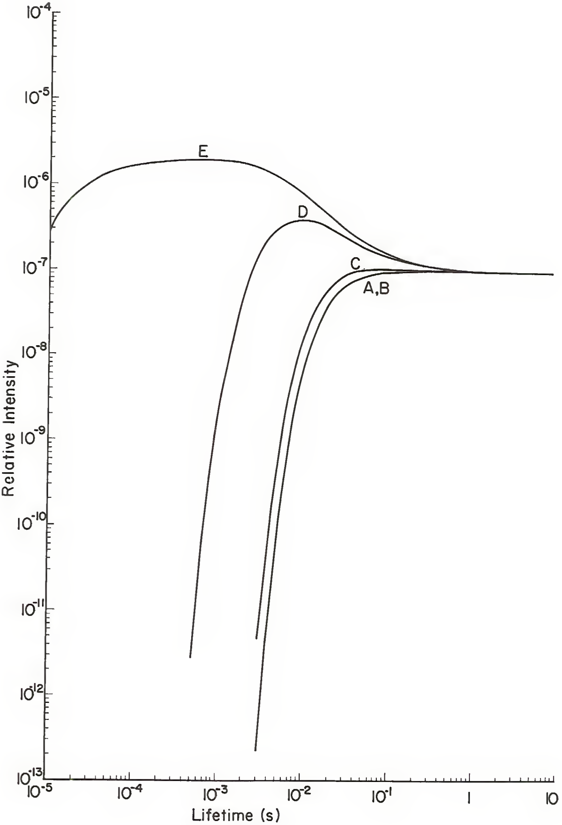
Relative Intensity
10^-4
10^-5
10^-6
10^-7
10^-8
10^-9
10^-10
10^-11
10^-12
10^-13
10^-5
10^-4
10^-3
10^-2
10^-1
1
10
Lifetime (s)
E
D
C
A,B

Figure 10. Response profile ($t_g = 5 \times 10^{-3}$s, f = 50 Hz).

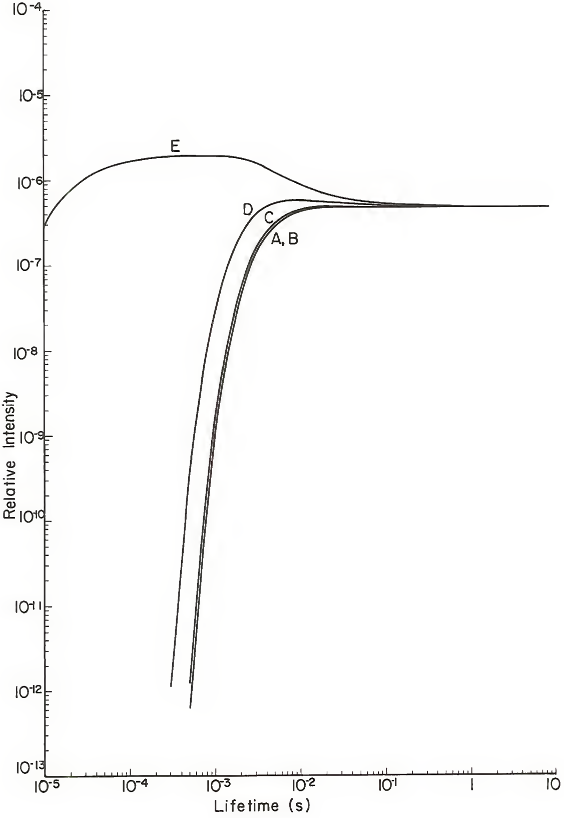
10^-4
10^-5
10^-6
10^-7
10^-8
10^-9
10^-10
10^-11
10^-12
10^-13
Relative Intensity
10^-5
10^-4
10^-3
10^-2
10^-1
1
10
Lifetime (s)
E
D
C
A, B

Figure 11. Response profile ($t_g = 5\text{x}10^{-3}$s, f = 100 Hz).

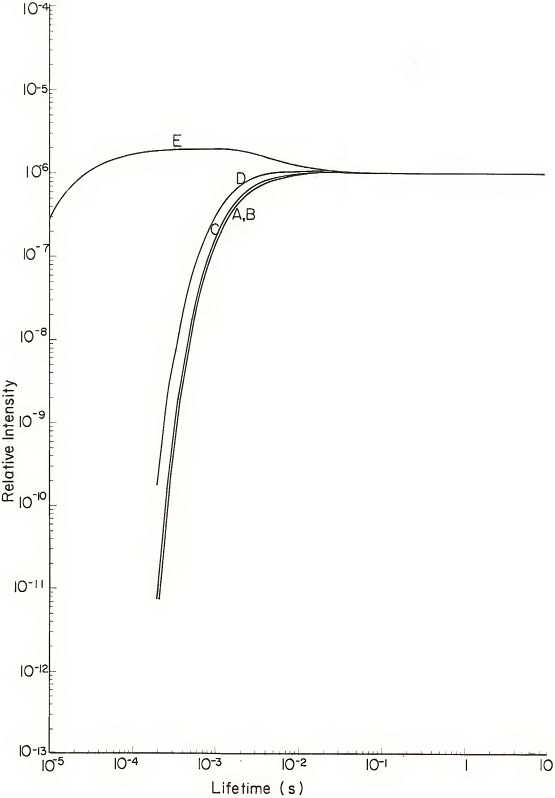

Relative Intensity
Lifetime (s)
10^-4
10^-5
10^-6
10^-7
10^-8
10^-9
10^-10
10^-11
10^-12
10^-13
10^-5
10^-4
10^-3
10^-2
10^-1
1
10
E
D
A,B
C

Figure 12. Response profile ($t_g = 5\text{x}10^{-4}$s, f = 1 Hz).

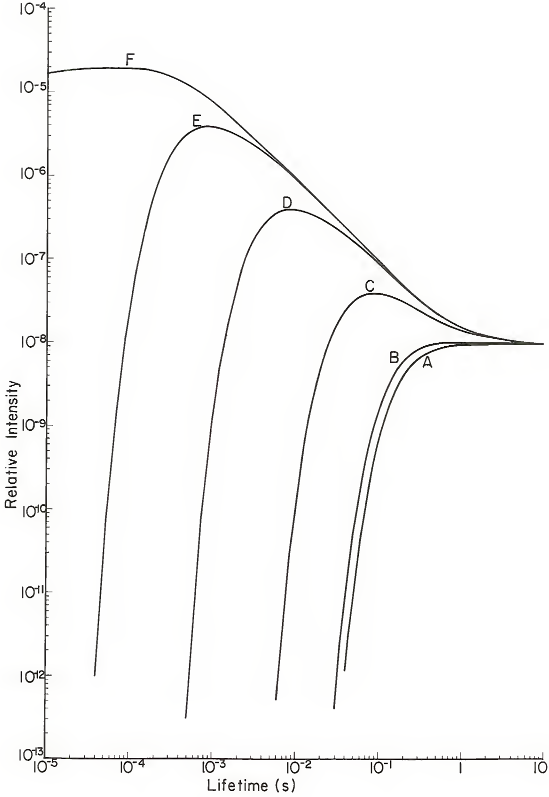
Relative Intensity
10^-4
10^-5
10^-6
10^-7
10^-8
10^-9
10^-10
10^-11
10^-12
10^-13
Lifetime (s)
10^-5
10^-4
10^-3
10^-2
10^-1
1
10
F
E
D
C
B
A

Figure 13. Response profile ($t_g = 5x10^{-4}s$, f = 10 Hz).

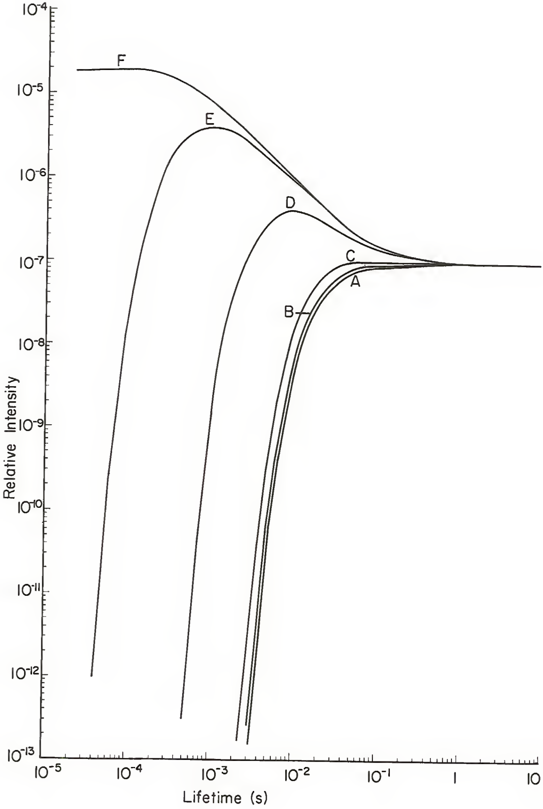
Relative Intensity
10^{-4}
10^{-5}
10^{-6}
10^{-7}
10^{-8}
10^{-9}
10^{-10}
10^{-11}
10^{-12}
10^{-13}
F
E
D
C
B
A
10^{-5}
10^{-4}
10^{-3}
10^{-2}
10^{-1}
1
10
Lifetime (s)

Figure 14. Response profile ($t_g = 5 \times 10^{-4}$s, f = 50 Hz).

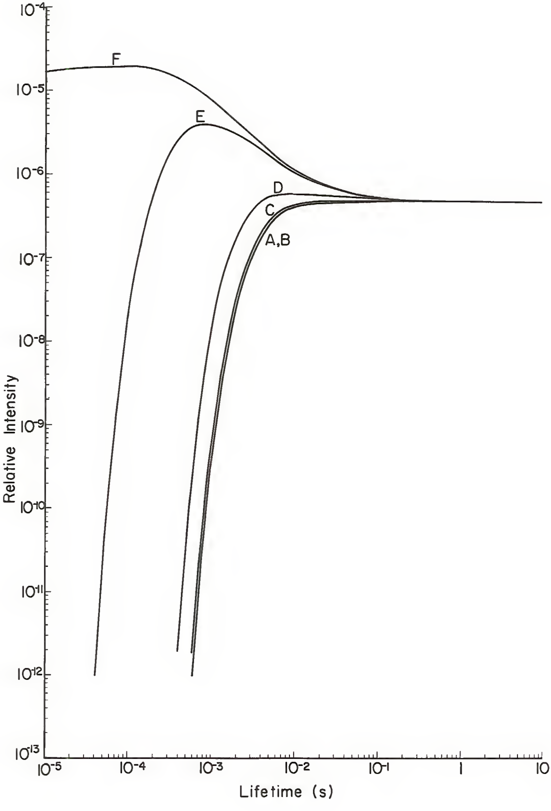
Relative Intensity
10^{-4}
10^{-5}
10^{-6}
10^{-7}
10^{-8}
10^{-9}
10^{-10}
10^{-11}
10^{-12}
10^{-13}
F
E
D
C
A,B
10^{-5}
10^{-4}
10^{-3}
10^{-2}
10^{-1}
1
10
Lifetime (s)

Figure 15. Response profile ($t_g = 5 \times 10^{-4}$s, f = 100 Hz).

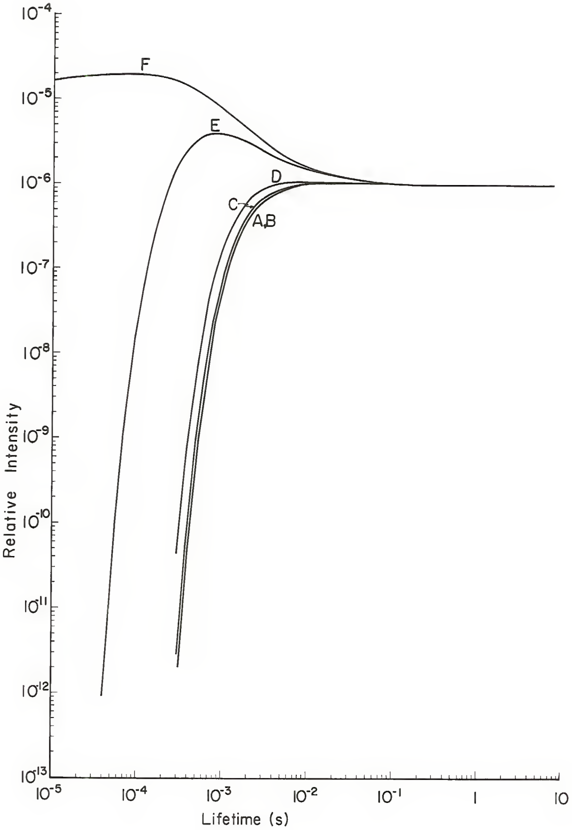
F
E
D
C
A,B
Relative Intensity
10^{-4}
10^{-5}
10^{-6}
10^{-7}
10^{-8}
10^{-9}
10^{-10}
10^{-11}
10^{-12}
10^{-13}
10^{-5}
10^{-4}
10^{-3}
10^{-2}
10^{-1}
1
10
Lifetime (s)

Figure 16. Response profile ($t_g = 5x10^{-5}$s, f = 1 Hz).

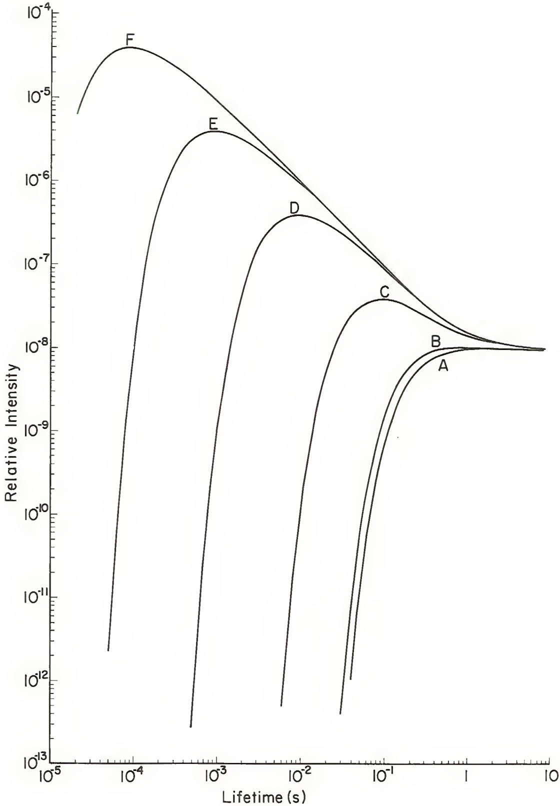
Relative Intensity
Lifetime (s)
10^{-4}
10^{-5}
10^{-6}
10^{-7}
10^{-8}
10^{-9}
10^{-10}
10^{-11}
10^{-12}
10^{-13}
10^{-5}
10^{-4}
10^{-3}
10^{-2}
10^{-1}
1
10
A
B
C
D
E
F

Figure 17. Response profile ($t_g = 5\mathrm{x}10^{-5}$s, f = 10 Hz).

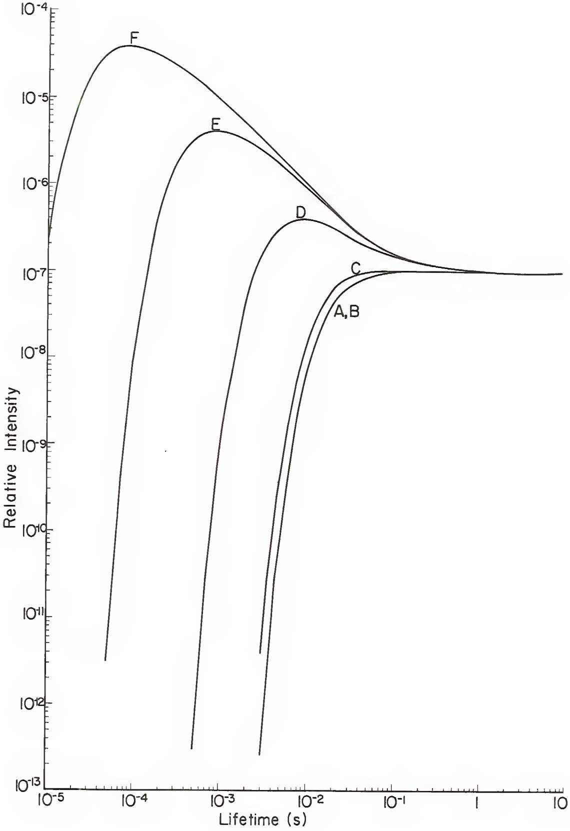
10⁻⁴
10⁻⁵
10⁻⁶
10⁻⁷
10⁻⁸
10⁻⁹
10⁻¹⁰
10⁻¹¹
10⁻¹²
10⁻¹³
Relative Intensity
10⁻⁵
10⁻⁴
10⁻³
10⁻²
10⁻¹
1
10
Lifetime (s)
F
E
D
C
A,B

Figure 18. Response profile ($t_g = 5x10^{-5}s$, f = 50 Hz).

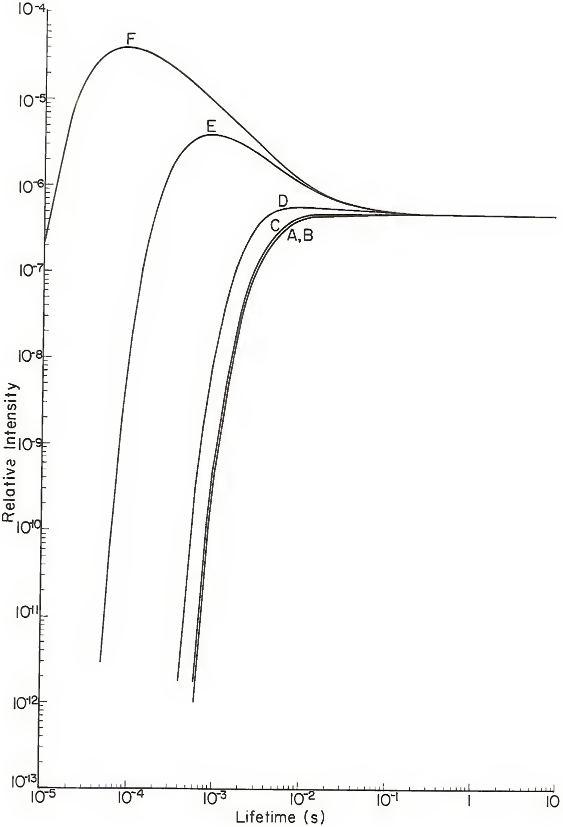

Relative Intensity
10^{-4}
10^{-5}
10^{-6}
10^{-7}
10^{-8}
10^{-9}
10^{-10}
10^{-11}
10^{-12}
10^{-13}
F
E
D
C
A,B
10^{-5}
10^{-4}
10^{-3}
10^{-2}
10^{-1}
1
10
Lifetime (s)

Figure 19. Response profile ($t_g = 5\mathrm{x}10^{-5}\mathrm{s}$, f = 100 Hz).

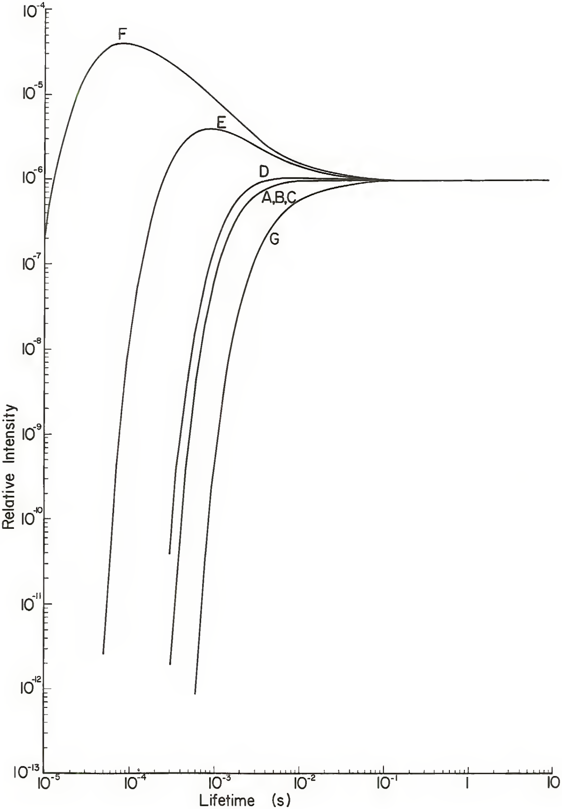
Relative Intensity
10^{-4}
10^{-5}
10^{-6}
10^{-7}
10^{-8}
10^{-9}
10^{-10}
10^{-11}
10^{-12}
10^{-13}
Lifetime (s)
10^{-5}
10^{-4}
10^{-3}
10^{-2}
10^{-1}
1
10
F
E
D
A,B,C
G

Results and Discussion

Initially, one figure will be discussed, before comparisons are made from figure to figure. Figure 8 shows the response for $t_g = 5\text{x}10^{-3}$s and f = 1 Hz. It is evident that the intensity enhancement at the maximum increases as the τ_{max} decreases. That is, as one goes from A, optimized for $\tau = 9$s, towards E, optimized for $\tau = 9\text{x}10^{-4}$s. Curve A has a very broad, flat maximum, while curve E has a very sharp, well pronounced peak. It is important to note that $(t_d)_{opt}$ is not the t_d of maximum attainable intensity. In all cases, decreasing t_d gives increased intensity, but simultaneously increases response to shorter lived components.

As mentioned earlier, the degree of enhancement (or discrimination) for phosphors of various lifetimes can be estimated by comparing their relative intensities. It can be seen that in all cases, except for lifetimes lying very closely together, discrimination over shorter lived components, $I_{T_{max}}/I_{T_S}$, is drastic. The reason for this is simply that the chosen delay time is so long that phosphorescence intensity due to shorter lived species has decayed significantly before the gate opens to sample the intensity. At longer lifetimes, the relative intensities approach the previously described limit of $t_p f$, which is 10^{-8} for Figure 8. It is obvious that, since the intensity contributions from long-lived components never drop below this level, in most cases, the ratio of $I_{T_{max}}/I_{T_{long}}$ will be substantially less than the ratio of $I_{T_{max}}/I_{T_{short}}$. This occurs because, regardless of where the gate is positioned for measurement of intensity from a particular lifetime component, the intensity resulting from phosphors of longer lifetime will always be present, and will always underlie the intensity decays for short-lived components.

Effect of excitation pulse width, t_p

The effect of t_p is not illustrated directly in any of the figures, because the earlier assumption concerning the relative magnitude of t_p makes it a strictly multiplicative factor in all cases presented here. The relative intensity is directly proportional to t_p, as long as $t_p << \tau$. This simple dependency is deceptive, however. The t_p factor enters the intensity expression as the term describing phosphorescence growth during the pulse, $[1-\exp(-t_p/\tau)]$. Within the limit of $t_p << \tau$, this growth term reduces to $I = I_0 t_p/\tau$. This growth factor is solely responsible for the observed intensity enhancement of short over long lifetime components.

At a fixed t_p, the phosphorescence intensity level attained due to growth during t_p is inversely proportional to the phosphorescence lifetime, τ. Therefore, for two components of identical I_0, the component of shorter lifetime is excited to a greater fraction of I_0, and the intensity due to the shorter lived component immediately following the excitation pulse (I_{p_1} in Figure 2) is greater than that of the long-lived component. However, this intensity due to the short-lived component also decays more rapidly following t_p. Therefore, for some period of time immediately after the excitation pulse, the intensity contribution of the shorter lived component is greater than that due to any longer lived components. This is shown by the shaded area in Figure 20, which illustrates the phosphorescence intensity growth/decay for two phosphors of differing lifetime. Thus, the maxima in the instrumental response profiles occur because the shorter lived components actually do have greater intensity along the earlier portion of the emission decay curve.

If t_p is increased, all lifetime components attain a larger fraction of I_0. As t_p approaches τ in value, the multiplicative effect gradually becomes exponential. As t_p continues to increase, components with very short lifetimes will completely attain I_0, and further lengthening of t_p will not further increase the intensity due to those components. However, longer lived components will still increase in intensity with increasing t_p, until the pulse width is so long that they too attain I_0. This is, of course, what occurs in a CW system, and $I/I_0 = 1$ for all lifetimes. Therefore if t_p is large, and all components reach I_0 during the excitation pulse,

Figure 20. Schematic representation of phosphorescence growth during the excitation pulse for two phosphors with different lifetimes.

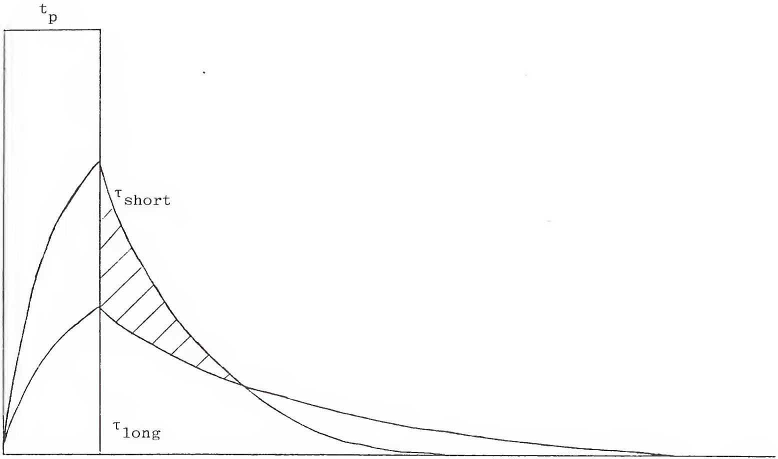
t_p
τ_{short}
τ_{long}

the intensity due to short-lived components will never be greater than that due to long-lived components, and the enhancement for τ_{max} over τ_{long} disappears.

Effect of gate width, t_g

The effect of gate width can be studied by examining the figures at fixed frequency. Figures 8, 12, 16; 9, 13, 17; 10, 14, 18; and 11, 15, 19 all exhibit the same trends. Gate width has no effect upon the curves for longer lifetime components (A-D). This is because $t_g << \tau$ and the two gate width dependencies in Equation 28 cancel each other. However, for shorter lifetimes (E,F), decreasing the gate width increases the intensity at τ_{max}, and thus the profile exhibits a much sharper maximum. There is then increased enhancement of the intensity at τ_{max} over other components, and increased or enhanced time resolution capabilities.

The effect of varying t_g is shown schematically in Figure 21. In the upper figure, a smaller segment of the emission decay curve is averaged, and the average intensity over the gate width more closely approximates the instantaneous intensity at any individual point. This is contrasted with the longer gate width shown in the lower figure. Note also that decreasing t_g at fixed t_d gives a higher average signal level. One could state that decreasing t_g enhances time resolution by increasing the number of resolution elements per unit time. However,

Figure 21. Schematic representation of the effect of gate width on observed phosphorescence signal.

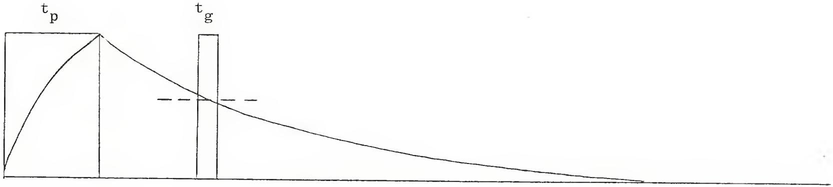
t_p
t_g

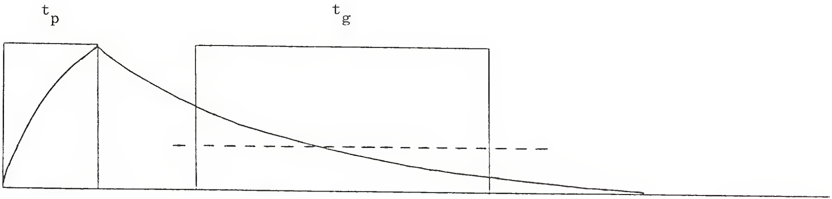
t_p
t_g

this increase in time resolution is had at the cost of increased OTC, and thus longer measurement time. Another result of decreasing t_g is that the optimum delay times for shorter and shorter lifetimes become available ($> 10^{-6}$s). Therefore, as t_g changes from 5×10^{-3}s to 5×10^{-5}s, the optimization curves for shorter lifetimes (F) appear.

Effect of repetition rate, f

The effect of repetition rate can be seen by fixing the gate width and varying f. Figures 8-11, 12-15, and 16-19 all demonstrate the same trends, but Figures 16-19 ($t_g = 5 \times 10^{-5}$s, f = 1, 10, 50, 100 Hz) are the most instructive.

(1) In the longer lifetime region, intensity is directly proportional to f, with the frequency dependence rapidly decreasing towards shorter lifetimes. This is due to the pulse-to-pulse intensity overlap or growth discussed earlier in this Chapter. The intensity observed during t_g is composed of phosphorescence decays resulting from a succession of excitation pulses. The amount of overlap between pulses is dependent upon the lifetime, which determines how rapidly the intensity decays, and the repetition rate, f, which determines the temporal spacing of the pulses. Figure 22 demonstrates the principle. In the upper sequence, 1/f is long compared to τ, and the intensity resulting from the first pulse

Figure 22. Schematic representation of the effect of frequency on pulse-to-pulse phosphorescence intensity growth.

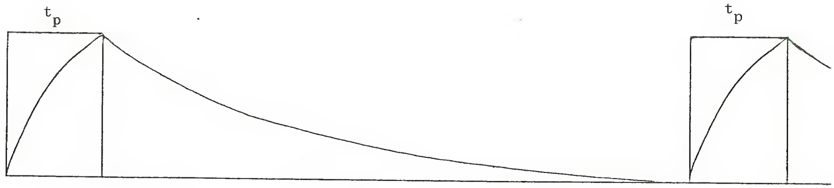
t_p
t_p

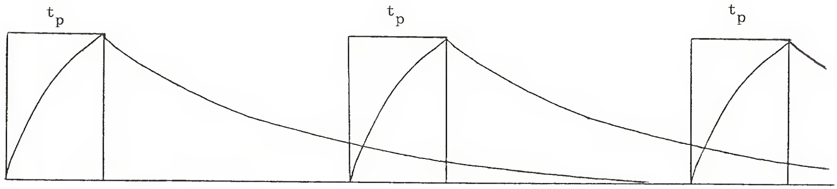
t_p
t_p
t_p

has disappeared before the second pulse occurs. Thus, there is no overlap, and the observed intensity results from only a single excitation pulse. It is also evident that frequency will show no effect as long as no overlap occurs. However, if the excitation pulses are placed closer together by increasing f, overlap begins to occur, and the observed intensity level increases. This is shown in the lower sequence of Figure 22. If $f\,\tau \geq 10$, the frequency dependence becomes multiplicative.

(2) As f increases, the limiting long lifetime intensity level extends to shorter lifetimes.

(3) The optimization curves representing longer lifetimes (A-C) converge as f increases. This is expected from the $(t_d)_{opt}$ plots, because increasing f moves $(t_d)_{opt}$ for those lifetimes into the asymptotic region. As the optimum delays become more similar, the response profiles converge. At 100 Hz (Figure 19), $(t_d)_{opt}$ is identical for curves A-C. Thus, as indicated in the earlier discussion, lifetimes lying in the asymptotic region can not be resolved at that set of experimental conditions.

(4) As f increases, the degree of enhancement of τ_{max} over τ_{long} decreases, because the intensity at longer lifetimes increases more rapidly than that at shorter lifetimes. Thus, increasing f gives greater intensity from long-lived components, but decreases the ability to resolve short-lived components in the presence of long-lived components.

(5) As f increases, the OTC, and thus the total measurement time, decreases.

Summary

The conclusions drawn from the preceding sections can be conveniently summarized.

(1) For any given set of experimental conditions, $(t_d)_{opt}$ can be calculated to position the maximum response at any given lifetime.

(2) The gate width, t_g, has no effect on the intensity observed from long-lived components; however, as τ decreases, decreasing t_g gives enhanced response to τ_{max}, but at the expense of longer measurement time. In addition, optimum delays for shorter lifetimes become available.

(3) The excitation pulse width, t_p, has a multiplicative effect for $t_p << \tau$, but the effect becomes exponential as t_p approaches τ in magnitude.

(4) Increasing the frequency, f, causes a proportional increase in intensity for long-lived components, with the frequency dependence decreasing towards shorter lifetimes. The limiting long lifetime intensity, ft_p, extends to shorter lifetimes, and the curves for optimizing longer lifetimes converge, so that long lifetimes can not be effectively resolved from one another. The enhancement factor $I_{\tau_{max}}/I_{\tau_{long}}$ also decreases, but the measurement time decreases.

The results of this chapter should have good applicability in the selection of experimental parameters for both conventional and time resolved phosphorimetric analysis. However, in applying these results to real systems, the limitations of the "real world" must be realized. These conclusions assume that the excitation pulse width, t_p, does not change with f, nor does the power per pulse or the pulse to pulse reproducibility (a severe noise source) change with f. If, for example, the reproducibility of power per pulse decreases as f increases, the actual measurement time may not decrease by the predicted amount, because a larger time constant may be required to compensate for the additional noise. Likewise, most pulsed sources exhibit lower power per pulse as f is increased. Therefore, a predicted intensity increase due to higher repetition rate may be proportionately less than expected, due to the loss of power per pulse.

Finally, it must be remembered that for the response profiles it was assumed that I_0 was constant. If, in a real mixture of components, one component has a hundred times greater I_0 than another component, a hundred-fold enhancement for the latter over the former will only equalize the actual measured intensities.

CHAPTER III
EXPERIMENTAL

It was decided that two different types of experiments would be performed. One set of measurements was designed to determine the validity of the theoretical work discussed in Chapter II, and consequently, the validity of the conclusions drawn concerning the effects of t_p, t_d, and f on the measured phosphorescence intensity. The second set of measurements used the guidelines established in Chapter II to select experimental conditions for the TRP analysis of two binary and one ternary mixtures of spectrally similar compounds. The experimental system and basic procedures used for these measurements are described in this Chapter.

Instrumentation

A block diagram of the experimental system is shown in Figure 23. The model numbers and manufacturers of the individual components are listed in Table 6. The system is very similar to that of Boutilier (30), and some component specifications are from his work.

The sample compartment, constructed of aluminum painted flat black, consisted of two mating sections. The lower section was designed to accommodate a Dewar

Figure 23. Block diagram of the experimental system.

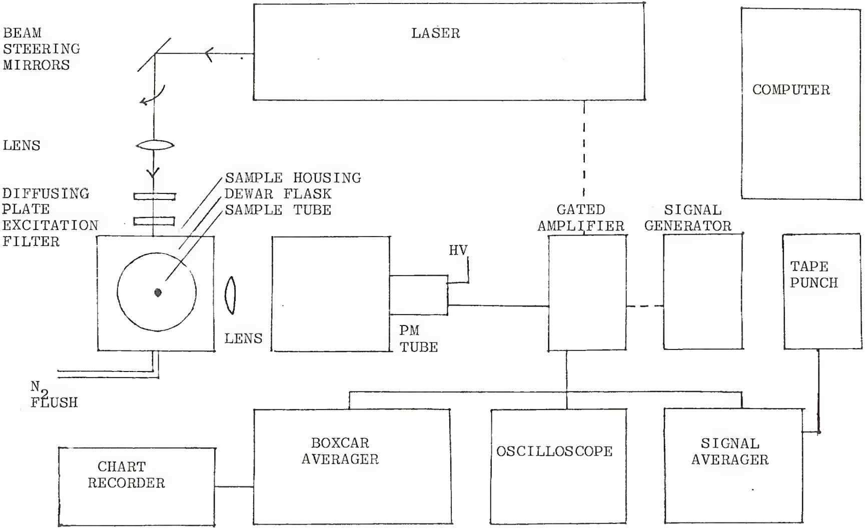
BEAM
STEERING
MIRRORS
LASER
COMPUTER
LENS
SAMPLE HOUSING
DEWAR FLASK
SAMPLE TUBE
DIFFUSING
PLATE
EXCITATION
FILTER
GATED
AMPLIFIER
SIGNAL
GENERATOR
HV
TAPE
PUNCH
LENS
PM
TUBE
N_2
FLUSH
CHART
RECORDER
BOXCAR
AVERAGER
OSCILLOSCOPE
SIGNAL
AVERAGER

TABLE 6
EXPERIMENTAL EQUIPMENT AND MANUFACTURERS

Item	Model Number	Source
Nitrogen laser	C950	Avco Everett Research Lab., Everett, MA
Monochromator	H-10	American ISA, Inc., Metuchen, NJ 08840
Photomultiplier tube	4837	RCA Corp., Lancaster, PA 17604
Photomultiplier housing	180	PAR Corp., Princeton, NJ 08540
High voltage power supply	EU-42A	Heath Co., Benton Harbor, MI 49022
Signal generator	110	Wavetek, Inc., San Diego, CA 92123
Oscilloscope	122AR	Hewlett-Packard, Palo Alto, CA 94306
Boxcar averager	CW-1	PAR Corp., Princeton, NJ 08540
Chart recorder	SRG	Sargent-Welch, Skokie, IL 60076
Signal averager	BIOMAC 1000	Data Lab., Ltd., Mitcham, Surrey, U. K.
X-Y recorder	Plotamatic 715	MFE Corp., Salem, NH 03079

flask, which possessed an optical tail. The flask was fitted with a Teflon collar, which fitted the flask snugly into position. The Dewar flask could be rotated to allow accurate repositioning each time it was removed for filling with liquid nitrogen. The lower section of the sample compartment was continuously flushed with dry nitrogen gas to minimize condensation on the viewing region of the Dewar flask. The upper section of the sample compartment was a cylindrical cover which fitted over the top of the Dewar flask and mated closely with the lower section. This section could be rotated with respect to the lower section. An NMR spinner was mounted on top of this cylinder. The sample cell was mounted in a cylindrical Teflon holder which slip-fit into the spinner. The spinner functioned only as a stationary positioning device.

The sample cell itself was a length of synthetic fused quartz tubing. Two sizes of tubing were employed: 2 mm id, 4 mm od (Thermal American Fused Quartz Co., Montville, NJ 07045); and precision bore 1 mm id, 3 mm od (Wilmad Glass Co., Inc., Buena, NJ 08310). The cell was fitted into the Teflon holder by wrapping with Teflon tape. The length of the cell was adjusted so that the excitation beam was centered approximately 0.5 in above the bottom of the cell, which was filled to a height of 1.0 in with the sample solution. The optimum rotational position of the upper section of the sample compartment had to be determined for each individual cell, because the quartz tubing was not usually straight.

The excitation source was an Avco nitrogen laser. The term "laser" is somewhat of a misnomer, as the nitrogen laser is actually a super-radiant source. The output beam consisted of two horizontal lines approximately 2 1/2 in wide separated by 1/8 in. The wavelength of primary lasing action is in the ultraviolet at 337.1 nm, with output bandwidth of <0.1 nm. The effective pulse width was 10 ns. The average power is specified as 100 mW, with peak output power of 100 kW. The repetition rate, f, is variable up to 100 Hz. All measurements were made with the laser pulsing repetitively at 15 torr of purified nitrogen gas and 15 kV high voltage.

During the course of experimentation, it became obvious that there was significant variation in laser power per pulse with change in f. Measurements were conducted to determine the relative loss in power with increasing repetition rate. A photodiode was first used to examine the shape of the pulse, but due to the very short duration of the pulse, no quantitative results were obtained. However, it was observed that the laser pulse shape was complex, and consisted of two overlapping temporal pulses. Then, a J3 Pyroelectric Joulemeter (Molectron Corp., Sunnyvale, CA) was employed to measure the dependence of energy per pulse with f. There was no measurable decrease in energy per pulse from 1 to 10 Hz, but there was a decrease of 14% at 50Hz, and of 38% at 100 Hz. In addition, it was found that the pulse-to-pulse reproducibility was much worse at 50 Hz than at any other repetition rate.

Because the long axis of the sample was oriented vertically, two front surface planar mirrors were used to rotate the laser output beam by 90%, thus insuring maximum spatial overlap between excitation beam and sample. The mirrors were mounted so as to allow height adjustment, and rotation of each mirror about two axes. The beam was focused on the sample by a 3 in diameter 8 in focal length lens. The minimum spot size was approximately 2 by 5 mm, due to the greater divergence along the long axis of the output beam. An interference filter with 10 nm bandwidth and peak transmittance of 42% at 340 nm was used to block the nonlasing nitrogen emission lines.

Preliminary work indicated that irreproducible positioning of the sample cell, coupled with the inherent random nature of the frozen sample matrix, caused major precision problems. This is common in phosphorimetry. In order to try to minimize these effects, a clouded quartz plate was inserted between the lens and the sample, in the hope that a more homogeneous excitation beam would result. In addition, the precision-bore 3 mm od cell was chosen for use, because it was straighter than the 4 mm od tubing. The smaller tubing was found to show no better precision, and eventually the 4 mm tubing was again employed, due to the larger signal levels attainable.

A 15 mm diameter 25 mm focal length quartz lens was used to form an image of the sample cell on the entrance slit of the monochromator. The monochromator was an f/3.5 0.1 m focal length, and was equipped with a concave holographic grating having reciprocal linear dispersion of 9 nm/nm. Two millimeter slits were used for intensity measurements giving a spectral bandpass of 16 nm.

The phosphorescence wavelength selected by the monochromator was detected by a photomultiplier tube in a light-tight compartment. The PMT was wired for fast response, and was operated at -800 V. Initially, an RCA 4837 PMT was used, but an 1P28 was used later in the measurements. The signal current from the PMT was amplified by a laboratory constructed (19,30) current-to-voltage (I-V) gated amplifier. The amplifier contained two stages of amplification, and the gating function grounded the input signal for a short period of time during and immediately after the excitation pulse. This prevented saturation of the amplifier due to the high fluorescence and scatter signal levels. The amplifier had two outputs. The first output was connected to either the oscilloscope or signal averager. The output is buffered, and smoothed the signal with an active low pass filter of variable time constant. In addition, a -3.00 V DC offset was added to allow maximum use of the available A/D dynamic range of the signal averager. The second output is also buffered, but not filtered, and was connected to the boxcar input. A function generator triggered the I-V amplifier, which contained circuitry that allowed it to trigger the remaining components, including boxcar, laser, and signal averager.

There were several problems involving this amplifier. First, a switching transient of large amplitude occurred when the amplifier gate opened. This could easily be stretched by the active filter, and thus interfered with lifetime measurements on the signal averager. It was necessary to very carefully adjust the time constant to provide some smoothing, but without distorting the decay curve. Secondly, the most sensitive gain setting was 3.02×10^{8} V/A, so that small signals were not easily measured. In addition, the amplifier showed serious drift in this range.

The boxcar averager used was the PAR Model CW-1. Some important specifications, as listed in manufacturer's literature (31) are as follows:

sensitivity: ±0.2 V to ± 100 V in 1-2-5 sequence;

time constant: 100 μs to 100 s in 1-3 sequence;

time base: 10 μs to 1 s in 1-2-5 sequence;

gate width: 1 μs to 110 ms (10% accuracy); and

delay time: 0 to 100% of time base (5% accuracy).

There are design limitations that prevented complete independence of f, t_g, and t_d. The output of the boxcar was plotted on a strip chart recorder.

Since it was necessary for many different lifetime measurements to be made in these studies, a multichannel signal averager was employed for lifetime determinations. The signal averager had 1000 channels, with total sweep times available in steps from 5 ms to 81.92 s. Delays could be introduced before and after the sweep. From 1 to 16,384 sweeps could be averaged (32). The emission decay curve stored in the signal averager memory was output to an X-Y recorder, yielding a plot of signal level versus time. The time axis was calibrated with respect to the sweep time setting. Boutilier (30) used a tape punch to transfer the data to a computer for least squares fitting, but due to computer malfunction, analog output was used in this work.

All components of the optical train were mounted solidly on optical benches. The sample compartment, optical components, monochromator, and PMT were enclosed in a flat black enclosure, designed to minimize stray light. Electrical components were grounded to an earth ground.

Reagents

All chemicals and drugs used in this study were reagent grade, and were used as received. Controlled substances were used in accordance with BNDD regulations. The reagents were obtained from the following sources:

chlorpromazine hydrochloride, Smith Kline and French Labs., Philadelphia, PA;

cinchonidine, vanillin, Sigma Chemical Corp., St. Louis, MO;

fluphenazine hydrochloride, perphenazine, Schering Corp., Kenilworth, NJ;

nupercaine hydrochloride,(cinchocaine hydrochloride), CIBA Pharmaceutical Co., Div. CIBA-GEIGY Corp., Summit, NJ;

papaverine hydrochloride, J. Hillis Miller Health Center, University of Florida, College of Pharmacy, Gainesville, FL;

quinine hydrochloride dihydrate, Aldrich Chemical Co., Inc., Milwaukee, WI;

thioridazine hydrochloride, Sandoz Pharmaceuticals, E. Hanover, NJ;

ethyl alcohol, U. S. Industrial Chemicals Co., New York, NY;

deionized water from a Barnstead Nanopure water system, Barnstead, Boston, MA.

Further information concerning the structures and applications of these compounds is readily available (33,34).

All glassware was cleaned by soaking in Nochromix (Godax Laboratories, New York, NY), followed by repetitive rinsing in first distilled water, then in Nanopure water. Stock solutions were prepared by weighing out the desired quantity on a Perkin-Elmer Model AM-2 Autobalance

(Perkin-Elmer, Norwalk, CT), and diluting with the premixed solvent in a volumetric flask. The two solvent mixtures used were 30%/70% and 40%/60% (V/V) ethanol/water. Dilutions were prepared in 10 ml volumetric flasks, with the aid of a micropipette (Oxford Sampler Micropipetting System, Oxford Lab., Foster City, CA). Solutions were protected from light whenever possible and were used soon after preparation.

Instrumental Procedure

All intensities were determined from the chart recorder tracing obtained from the boxcar averager. The monochromator slit width was 2.0 mm for intensity measurements, and either 0.5 or 1.0 mm for spectral scans.

For lifetime measurements, the oscilloscope trace was used to approximate the sample lifetime, and the signal averager sweep time was set to a value that would allow the phosphorescence intensity to decay away completely during the sweep. The active filter on the amplifier was adjusted to provide some smoothing (increased SNR), but to avoid distorting the decay curve. For phosphors with lifetimes short enough to allow the total sweep time to be less than 1 s, the repetition rate was 1 Hz, and 32 sweeps were averaged. For longer lifetimes, the same procedure was followed at smaller repetition rates. However, if the signal level was too small under these conditions, the sample was irradiated at a fixed rate (10-20 Hz) to allow some higher steady state intensity level to be reached. Then, the excitation was blocked, and the emission decay curve measured over only one sweep. Of course, the SNR ratio was poorer, due to the fact that no averaging was used. The intensity versus time information was recorded on graph paper. The time axis was calibrated by dividing the total number of graph units by the sweep time.

Lifetimes were calculated from the graphs by taking the signal level at a point near the start of the decay, and determining the period of time required for that signal level to decay to 1/e (0.368) of its initial value. Then, the value of 2 x τ was calculated by determining the time required for the decay to reach 2/e (0.135) of the initial value, and the two lifetimes determined from each plot were averaged. Normally, three decays were plotted for each sample, and the six calculated lifetimes were averaged. The average precision for lifetime measurements was approximately $\leq$ 5% RSD.

Sampling Procedure

Phosphorimetry has suffered from poor precision (∿ 10% RSD), caused in large part by problems associated with the liquid nitrogen. These included bubbling, ice crystal formation, and condensation on the viewing region of the Dewar flask. However, the most serious problem is the irreproducibility of the freezing process itself. Depending upon the solvent, the frozen matrix might be a clear glass, a cracked glass, a snow, or something in between. In addition, bubbles sometimes formed in the sample plug in the viewing area. Even for one particular analyte/solvent combination, the characteristics of the rigid matrix can vary with the nitrogen level, rate of cooling, etc.

In order to attempt to minimize those effects, preliminary experiments were performed, in which solutions of nupercaine HCl in various solvent compositions were frozen by a variety of procedures. Several results arose from this work: the precision was almost identical for solvent compositions of water with 10-40% ethanol, although the nature of the matrix changed; bubble formation in the sample cell was found to be due to the sample solution rising in the cell because of cooling of the air above the sample plug in the cell; and the height of nitrogen in the Dewar was critical.

Based on these observations, a standardized sampling procedure was adopted. In addition, the quartz diffusing plate was added to the optical train, and the 3 mm od precision bore tubing was chosen for use. Between samples, the cell was rinsed well with pure water, blown dry with compressed air, and dried externally with paper wipers. The Dewar flask was filled with liquid nitrogen to approximately 1 in from the top. The sample cell was inserted into the upper section of the sample compartment. By a pipetting technique, the lower 1 in of the cell was filled with solution, and the outside dried. The solution was allowed to form a convex surface on the bottom edge of the tube. This tended to minimize bubble formation.

Handling as a unit the combination sample cell/sample compartment allowed the freezing process to be viewed directly. The lower tip of the sample cell was held just above the liquid nitrogen, so that the cold vapors froze the sample more slowly than direct immersion. As the frozen area moved up the sample, the tube was gradually immersed. Once the entire sample was frozen, the upper compartment was fitted into place, and was rotated to the optimum position.

Due to its enhanced ability to dissolve the types of compounds used in this work, 40%/60% ethanol/water was initially chosen as the solvent. This solvent mixture normally yielded a cracked glass matrix. After several weeks of experimentation, however, it was found that the matrix sometimes formed a clear glass, which gave different lifetimes and intensities. Investigation of this phenomenon indicated that this was due to an unexpected effect. Throughout the course of each day, as the Dewar flask was refilled many times, the temperature of the sample compartment gradually decreased.

Eventually, the Dewar flask and its surroundings became cold enough so that the liquid nitrogen ceased bubbling (and later superheated). Since the cold nitrogen gas was the agent responsible for freezing the sample, the difference in boil off rate changed the rate of freezing. Because the preliminary investigations had demonstrated that the 30%/70% solvent mixture formed a milky matrix (instead of a glass), further studies on the 30%/70% mixture were performed. These studies demonstrated that the 30%/70% mixture was less susceptible to changes in the rate of cooling than was the 40%/60% mixture, and therefore the former was employed for all further investigations.

CHAPTER IV
RESULTS AND DISCUSSION

As a preface to the primary experimentation, it was necessary to collect a series of compounds which would phosphoresce when excited by the nitrogen laser at 337.1 nm. A large number of compounds were surveyed. Those indicating sufficient phosphorescence intensity levels were subjected to preliminary lifetime measurement. The results of these preliminary measurements are shown in Table 7. The compounds used in further work were selected from this list.

Validation of Theoretical Analysis

The first measurements were designed to test the validity of the conclusions drawn in Chapter II. If any theoretical work is to have much practical applicability, at the very minimum, the trends predicted by theory must agree with those observed experimentally. Although it would be very difficult to reproduce experimentally plots such as those in Figures 8-19, it is possible to measure the relative changes in phosphorescence intensity with t_d, t_g, and f for several phosphors of different lifetimes, and to compare these with the relative changes predicted by theory. Because the excitation pulse width,

TABLE 7
PRELIMINARY LIFETIME MEASUREMENTS

Compound	Classification	Lifetime	Emission Wavelength (nm)	Concentration (ppm)
chlorpromazine HCl	tranquilizer	66.5 ms	487	57
cinchonidine	antimalarial	1.15 s	497	201
fluphenazine HCl	tranquilizer	56.5 ms	495	50
nupercaine HCl	local anesthetic	1.08 s	482	101
papaverine HCl	muscle relaxant, antispasmodic	1.87 s	482	46
perphenazine	tranquilizer	63.7 ms	490	53
quinine HCl-$2H_2O$	antimalarial	0.809 s[a]	518	107
thioridazine HCl	tranquilizer	56.0 ms	486	75
vanillin	flavoring agent, clinical reagent	0.220 s	486	221

Notes: The solvent was 40/60 (V/V) ethanol/water. The signal level of the blank was negligible. λ_{EX} = 337.1 nm

[a] Lifetime measured at 486 nm

t_p, is fixed by the nitrogen laser at 10^{-8}s, the parameters to be studied for each lifetime were gate width, delay time, and repetition rate. A total factorial design for these three factors at four levels would require 64 separate measurements for each phosphor. Instead, a partial factorial design was selected. The four levels for each factor were chosen so that the values would cover a wide range. Selecting the values was very complex, due to the theoretical and instrumental limitations on the independence of t_g, t_d, and f. The values chosen for repetition rate were 1, 10, 50, and 100 Hz; and for gate width and delay time, 10^{-1}, 10^{-2}, 10^{-3}, and 10^{-4}s. Of the 64 possible combinations, 26 were physically impossible ($t_d + t_g > 1/f$) and 5 were instrumentally impossible (time base not < 1/f). Eventually, 16 combinations were chosen for the actual measurements. One set of conditions was chosen as a reference, to which all other measurements were ratioed. This would then yield relative intensity changes. Three measurements per factor measured primary effects (i.e., f alone, t_d alone, and t_g alone), while two measurements were assigned to each binary interaction (f and t_g, t_d and t_g, f and t_d). The sets of parameters were numbered to allow easier comparison of data. Table 8 lists the 16 measurements.

Three different phosphors were chosen for these studies. The solutions were prepared at fairly high concentrations, to insure large signal levels.

TABLE 8
PARAMETERS FOR EXPERIMENTAL VALIDATION

Measurement Number	Effect Studied	f (Hz)	t_g (s)	t_d (s)
1	-	1	10^{-3}	10^{-3}
2	t_d	1	10^{-3}	10^{-1}
3	t_d	1	10^{-3}	10^{-2}
4	t_d	1	10^{-3}	10^{-4}
5[a]	t_g	1	10^{-1}	10^{-3}
6	t_g	1	10^{-2}	10^{-3}
7	t_g	1	10^{-4}	10^{-3}
8	f	10	10^{-3}	10^{-3}
9	f	50	10^{-3}	10^{-3}
10	f	100	10^{-3}	10^{-3}
11	t_g, t_d	1	10^{-4}	10^{-2}
12	t_g, t_d	1	10^{-1}	10^{-1}
13	f, t_d	10	10^{-3}	10^{-2}
14	f, t_d	100	10^{-3}	10^{-4}
15	f, t_g	100	10^{-4}	10^{-3}
16	f, t_g	10	10^{-2}	10^{-3}

[a] Actual delay was $2\text{x}10^{-3}$

Nupercaine HCl is a local anesthetic with maximum emission at 482 nm, and a lifetime of 1.08 s in the 101 ppm solution used here. The second solution was 221 ppm vanillin, a flavoring agent and clinical reagent, with a lifetime of 0.220 s at 486 nm. The third solution was 75 ppm thioridazine HCl, a tranquilizer, with a lifetime of 56.0 ms at 486 nm.

In order to minimize errors introduced by sample-to-sample imprecision and excessive laser flicker noise (drift), measurement #1 was taken as a reference intensity. With the laser warmed and running continuously, the sample was frozen and positioned. The instrumentation was set to correspond to measurement #1. The excitation beam was allowed to strike the sample, and the measurement was begun by DC coupling the boxcar input. The time constant was adjusted to yield a compromise between OTC and SNR. After the required measurement period, the excitation beam was blocked (to avoid unnecessary sample decomposition), and the controls set to another measurement point. Measurement #1 was repeated after every other measurement. This made it possible to check for excessive sample decomposition, laser drift, nitrogen bubbling, or other effects. If the reference measurements before and after any point showed large variations, the measurement was repeated. Because the SNR varied somewhat with time and repetition rate, the time constant sometimes had to be adjusted to insure approximately the same SNR. Samples and liquid nitrogen were changed when increased noise or decreased signal level occurred.

The results were calculated by first converting each intensity measurement back to original PMT current (multiplying by recorder sensitivity and dividing by amplifier gain in V/A). The reference signal levels (measurement #1) before and after each measurement were averaged, and the intensity of the measurement ratioed to this value. Thus, the net result was a series of experimental signal ratios, all referenced to measurement #1.

The theoretically predicted ratios were calculated by using Equation 28, along with the particular t_d, t_g, and f, and lifetime, to calculate I/I_o under each set of conditions given in Table 8. Every value was ratioed to I/I_o for measurement #1, thus giving a set of experimental ratios predicted from Chapter II. If theory and experiment yielded the same relative intensity changes, the ratios would be identical.

Blanks were run for these measurements, but in most cases, the analyte signal levels were so large that the blank values were insignificant. The few cases where the blank correction was necessary are noted. The effect of loss of laser power with increasing repetition rate was corrected for by multiplying the theoretical ratios by 0.86 for 50 Hz measurements, and 0.62 for 100 Hz measurements. The results are presented in Tables 9-11.

A theory/experiment ratio of unity indicated perfect correlation. A ratio of less than unity indicated that the experimental change was larger than predicted; a ratio of greater than unity, indicated that the experimental change was less than predicted. The average agreement for the effect of t_d can be seen by averaging the three measurements in which only t_d is varied, and likewise for the other primary and binary effects. These average results for all three phosphors are listed in Table 12.

The ratios for the shortest lifetime phosphor, thioridazine HCl, are all slightly less than unity, except for the effect of t_g. The single worst point was #12, which can be attributed to the exteremly low signal level present under that set of conditions. In general, the relative intensity changes are slightly larger than predicted.

The results for vanillin are scattered, with some ratios less than unity, some greater. The effect of frequency is greater than predicted, while that of gate width is slightly less than predicted (except when it is paired with a change in frequency).

The longest lived phosphor, nupercaine HCl, shows the most pronounced deviation between theory and experiment. The effect of frequency falls short of the predicted change in each case. It is important to note, however,

TABLE 9
COMPARISON OF THEORETICAL AND EXPERIMENTAL INTENSITY RATIOS FOR THIORIDAZINE HCl
(τ = 56.0 ms, 75 ppm, 486 nm, 40/60 ethanol/water)

Measurement Number	Theory	Experiment	Theory/ Experiment
1	-	-	-
2	0.171	0.186	0.919
3	0.851	0.842	1.01
4	1.02	1.10	0.927
5	0.470	0.432	1.09
6	0.925	0.914	1.01
7	1.01	1.05	0.962
8	1.20	1.24	0.968
9	2.86	2.76	1.04
10	3.78	3.95	0.957
11	0.856	0.851	1.01
12[a]	8.05×10^{-2}	9.04×10^{-2}	0.890
13	1.02	1.05	0.971
14	3.85	3.96	0.972
15	3.81	3.98	0.957
16	1.11	1.12	0.991

[a] Extremely low signal level, required black correction

TABLE 10
COMPARISON OF THEORETICAL AND EXPERIMENTAL INTENSITY RATIOS FOR VANILLIN
(τ=0.220 s, 221 ppm, 486 nm, 40/60 ethanol/water)

Measurement Number	Theory	Experiment	Theory/ Experiment
1	-	-	-
2[a]	0.638	0.651	0.980
3	0.961	0.951	1.01
4	1.00	1.01	0.990
5	0.807	0.698	1.16
6	0.980	0.929	1.05
7	1.00	1.00	1.00
8	2.72	3.26	0.834
9	9.80	9.87	0.993
10	13.9	14.5	0.957
11	0.963	0.944	1.02
12	0.513	0.419	1.22
13	2.61	3.20	0.816
14	13.9	13.7	1.01
15	13.9	14.0	0.993
16	2.65	2.80	0.946

[a] Run on an identical solution at a later date

TABLE 11
COMPARISON OF THEORETICAL AND EXPERIMENTAL INTENSITY RATIOS FOR NUPERCAINE HCl
(τ = 1.08 s, 101 ppm, 482 nm, 40/60 ethanol/water)

Measurement Number	Theory	Experiment	Theory/ Experiment
1	-	-	-
2	0.915	0.895	1.02
3	0.993	0.943	1.18
4	1.00	0.984	1.02
5	0.954	0.903	1.06
6	0.993	1.06	0.937
7[a]	1.00	1.04	0.962
8	6.86	6.55	1.05
9	28.3	21.9	1.29
10	40.5	31.9	1.27
11	0.993	0.930	1.07
12	0.876	0.860	1.02
13	6.80	5.66	1.20
14	40.5	31.1	1.30
15	40.5	31.5	1.29
16	6.80	5.72	1.19

[a] Run on an identical solution at a later date

TABLE 12
AVERAGE RESULTS OF INTENSITY MEASUREMENTS FOR THREE PHOSPHORS

	Average Theory/Experiment Ratios		
Effect Studied	thioridazine HCl	vanillin	nupercaine HCl
t_d	0.952	0.993	1.07
t_g	1.02	1.07	0.986
f	0.988	0.928	1.20
t_g, t_d	0.950	1.12	1.04
f, t_d	0.972	0.913	1.25
f, t_g	0.974	0.970	1.24

that the magnitude of the relative changes in intensity with frequency are much larger for this longer lived phosphor than for either of the others.

In summary, the correlation of theory and experiment is remarkably good for all parameters and all three phosphors. Theory/experiment ratios range from 0.816 to 1.30, with the error increasing as the magnitude of the intensity change increases. There are a number of error factors present that could easily account for the observed deviation:

(i) The excitation pulse is not a rectangular block of energy as assumed in the model, but is rather a complex pulse consisting of two temporal lobes;

(ii) Although the net loss of power with increasing frequency was corrected for, changes in the laser pulse shape with f were not considered;

(iii) All of the noise sources inherent in immersion cooling were present, compounded with severe laser flicker noise which could easily amount to ± 15% of the observed signal level from one sample over a short period of time (5-10 minutes);

(iv) The specified accuracy for delay time and gate width was 5% and 10%, respectively;

(v) The assumption was made that the phosphorescence decay and growth lifetimes are equal ($\tau = \tau^R$), although the intense laser irradiation could be expected to cause them to differ;

(vi) Absolute errors in the measured lifetimes would cause error, in spite of the good precision of the lifetime determination.

The author was interested in seeing if the previously discussed pulse-to-pulse phosphorescence intensity growth could be recorded. This would enable one to observe qualitatively what happens when a series of excitation pulses impinges upon a non excited sample. This was relatively easy to record, and the same solutions of nupercaine HCl, thioridazine HCl and vanillin used in the previous experiments were also used here. All that was necessary was to set the signal averager for a relatively long sweep, set it to measure only one sweep, start the sweep, and then start the excitation. Thus, an intensity versus time plot was obtained which showed clearly the effect of the individual excitation pulses. These "growth profiles" were taken at several different repetition rates, since the amount of time required to reach the steady state should depend only on the sample lifetime, and not on f. A few of these growth profiles are shown in Figures 24-28. Figures 24-26 are for thioridazine HCl at 1, 10, and 100 Hz, while Figures 27-28 are nupercaine HCl at 10 and 100 Hz. It should be noted that the gains had to be changed when going to the higher repetition rates, and also that the nupercaine solution showed signs of decomposition on the date these were plotted, and the lifetime may differ slightly from the 1.08 s stated.

In Figure 24, the time period between pulses is so long that the intensity following each pulse decays away before the next pulse occurs. However, if the pulses are pushed closer and closer together (Figures 25, 26), some intensity remains at the start of the next

Figure 24. Growth profile for thioridazine HCl at 1 Hz (t = 56.0 ms, 5.12 s scan).

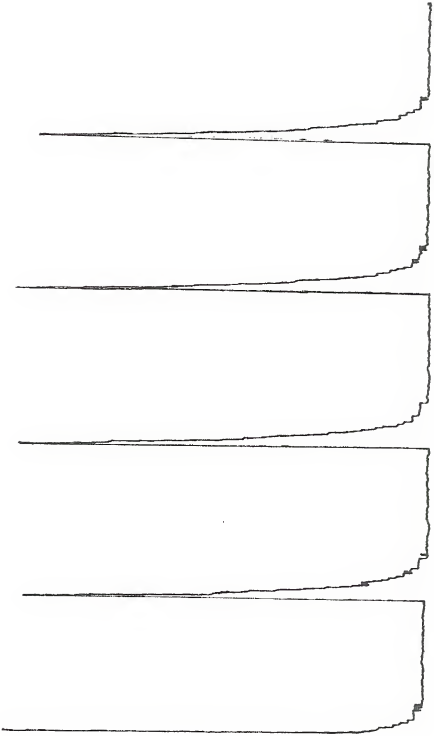

Figure 25. Growth profile for thioridazine HCl at 10 Hz (t = 56.0 ms, 0.640 s scan).

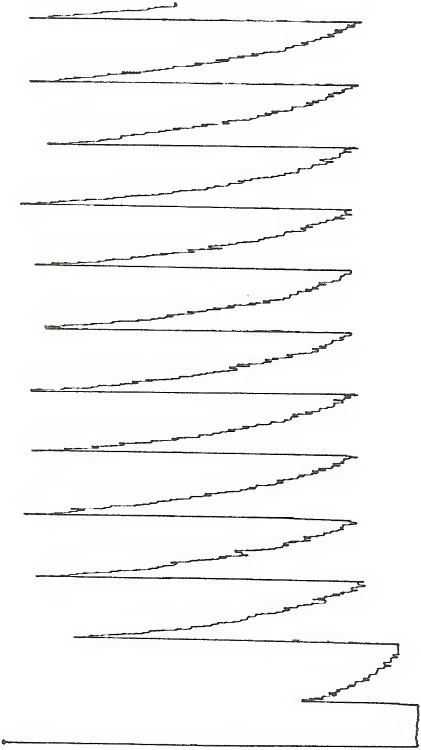

Figure 26. Growth profile for thioridazine HCl at 100 Hz (t = 56.0 ms, 0.640 s scan).

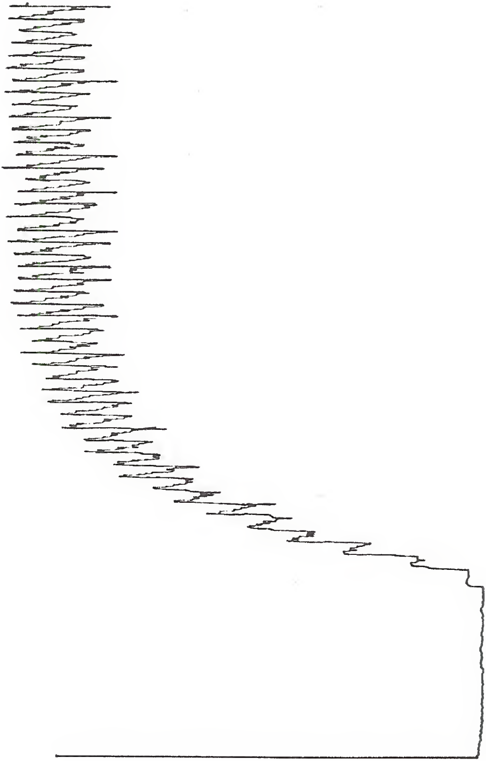

Figure 27. Growth profile for nupercaine HCl at 10 Hz (t = 1.08 s, 10.24 s scan).

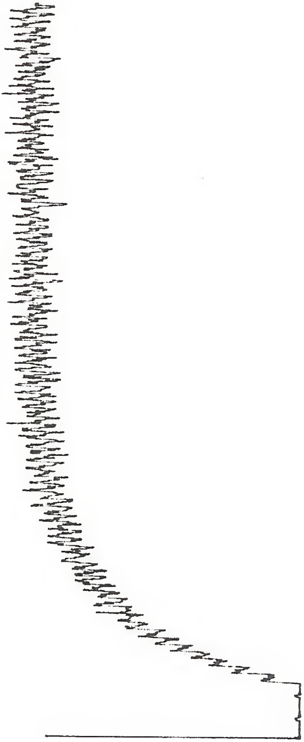

Figure 28. Growth profile for nupercaine HCl at 100 Hz ($t = 1.08$ s, 10.24 s scan).

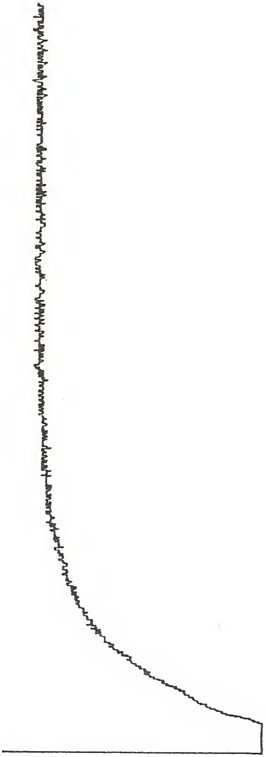

pulse, and the intensity level begins to increase. Note that the intensity reaches a steady state after some number of pulses. Figures 25 and 26, at different repetition rates but identical scan times, demonstrate that the time required to reach steady state is roughly identical for both Figures. This is also apparent in figures 27 and 28, where both figures show the growth for nupercaine HCl at the same scan time but different repetition rates. Although these measurements were qualitative, rough calculations demonstrated that the growth towards steady state occurred at a rate proportional to the sample lifetime, and that the curves roughly ($\sim$20%) fit the function $[1-\exp(-t/\tau)]$.

Therefore, based on the evidence presented in this section, the theoretical approach of Chapter II has been shown to agree quite well with experimental data, correctly predicting the direction and magnitude of changes in phosphorescence intensity with gate width, repetition rate, delay time, and lifetime.

Time Resolution of Phosphor Mixtures

This section of measurements was designed to demonstrate how the conclusions drawn in Chapter II can be used to select experimental conditions for time resolved phosphoroscopic analysis of multicomponent mixtures, and the types of results that can be expected. Three different synthetic mixtures were analyzed: a two component mixture of phosphors with different lifetimes; a two component mixture of phosphors with similar lifetimes; and a three component mixture. In addition to approximating the concentrations of the components, the effect of preparing the calibration curves at different delay times was examined. Although each component has greater intensity at shorter delay times, one might expect the calibration curve prepared at $(t_d)_{opt}$ for that component to provide good results. By estimating mixture concentrations from a series of calibration curves, it should be possible to see if there is any significant difference in the results obtained at different delay times.

The selection process for choosing experimental conditions is discussed separately for each mixture. The basic experimental procedure was the same for all mixtures. For each phosphor, solutions of 0.1, 0.3, 1, 3, 10, and 30 ppm were prepared by dilution from a 100 ppm stock solution. Prior to the analysis, the lifetime of each phosphor was carefully measured on a relatively dilute solution, usually 10 or 30 ppm. Based on these lifetimes, the experimental parameters were chosen. Calibration curves for each component were prepared by measuring the intensity for each dilution at the appropriate delay times (f and t_g fixed). Each solution was measured three times, and the results averaged. The time constant was chosen, and was not changed unless laser flicker noise changed drastically. Log-log plots of signal level (nA) versus concentration (ppm) were obtained and were blank corrected. The plots were fitted by a linear least-squares regression analysis on a Hewlett-Packard 25 programmable calculator, unless significant curvature was observed. The form of the fitted equation was

$$\log \text{nA} = (\log \text{ppm})a_0 + a_1 \tag{50}$$

with correlation coefficient r^2. Mixtures were prepared from the stock solutions. Each mixture was measured 8 or 16 times, and each replicate was quantitated at all of the required t_d's. The blank level was subtracted, the replicate values averaged, and % RSD calculated. The averaged total signal levels were input into the equations found in Tables 1 and 2, and the individual intensities calculated. The concentrations of the components were obtained by referring to the appropriate calibration curves. It should be noted that selection of experimental conditions relied upon previous lifetime measurements, while the lifetimes used in the data reduction were measured at the same time as the calibration curves were measured, and the values sometimes differed slightly.

Binary Mixture I

The first mixture analyzed contained two phosphors with significantly different lifetimes. The components were thioridazine HCl, with $\tau = 53.0$ ms at 30 ppm, and nupercaine HCl with $\tau = 1.19$ s at 10 ppm. By making the rough approximation that I_0 for both components in the mixture will be similar, Chapter II can be used to select t_d, t_g, and f for the measurements. For the results of the analysis to be accurate, the relative contributions of the two phosphors must be different at the two delay times, and the total intensity at the two times must also differ significantly.

In Figures 8-19, thioridazine HCl can be approximated (order of magnitude) by curves marked C, and nupercaine HCl by the curves marked B. The effect of gate width is negligible at these lifetimes in the range of gate widths studied, so a large value, 10^{-3}s, is chosen, to minimize the OTC. Figures 8-11 are plotted for $t_g = 5\text{x}10^{-3}$s, so these figures can be used to roughly represent the trends one would expect for $t_g = 10^{-3}$s. By referring to those figures, it is seen that B and C differ significantly at 1 and at 10 Hz, but that they converge at higher repetition rates. This is not desired, because the instrumentation will respond almost equally to both phosphors. The 10 Hz repetition rate will give a lower OTC than 1 Hz, with increased intensity from the longer lifetime component, but at the expense of pushing curves B and C closer together.

A better estimate of the relative response of the instrumentation for the two components can be obtained by calculating $(t_d)_{opt}$ for each component, choosing these as the two delay times at which the measurements should be made, and calculating I/I_0 for each component at both delay times. What one finds is that, for $t_g = 10^{-3}$, and f = 10 Hz, the two optimum delay times are 3.46×10^{-2}s and 4.88×10^{-2}s. The I/I_0 values indicate that at the shorter delay time, the enhancement ratio for thioridazine HCl over nupercaine HCl is 1.14, and at the second delay time, nupercaine HCl is enhanced by 1.14 over thioridazine HCl. However, the predicted total intensity difference at the two delay times is only 13%. Thus, we meet one requirement, but the total intensity change is probably marginal (of course, I_0 for the components will probably not be equal in the mixture, but the approach is useful).

Therefore, the frequency must be decreased to give a larger total intensity change (B and C are spread further apart), at the expense of a longer OTC. With $t_g = 10^{-3}$s and f = 5 Hz, the two optimum delay times are 4.78×10^{-2}s and 9.67×10^{-2}s. Now, the two enhancement ratios are 1.62 and 1.49, and the total intensity differs by 38%. We then expect the conditions set forth for multicomponent analysis to be met for this mixture under that set of experimental conditions. Similar reasoning was applied for the other mixtures, but less discussion will be required.

A summary of the experimental conditions and the results of the analysis appear in Table 13. This analysis yielded accurate concentration values for both components in both concentration ranges. The results for the shorter lived component are slightly low in both mixtures and both delay times, with larger error at t_{d_2}. Conversely, the concentrations measured from the longer lived component are slightly high in all cases, with less error in mixture IB, which contains the higher concentrations. The concentrations found for that component (B) are essentially the same at both delay times. In summary, then, the results for shorter lived thioridazine HCl are low and show greater error at the longer delay time, while the results for nupercaine HCl are high and show little difference at the two delay times.

Binary Mixture II

The second two component mixture contained two phosphors with very similar lifetimes: thioridazine HCl, with τ = 59.6 ms at 10 ppm (note difference in lifetime found in Binary Mixture I); and perphenazine, with τ = 72.7 ms at 10 ppm. This mixture is one that would push the capabilities of TRP to the limit, and was chosen for that purpose.

By studying Figures 8-19 and applying the procedure discussed a few pages earlier, t_g is again chosen as 10^{-3}s. However, for these phosphors, even at a low frequency

TABLE 13
ANALYSIS OF BINARY MIXTURE I

Component A: Thioridazine HCl $t = 53.0$ ms at 30 ppm

Component B: Nupercaine HCl $t = 1.19$ s at 10 ppm

$f = 5$ Hz, $t_g = 10^{-3}$s, $t_{d_1} = 4.78\text{x}10^{-2}$s, $t_{d_2} = 9.67\text{x}10^{-2}$s

486 nm, 40/60 ethanol/water

Calibration Curves

	t_d	a_o	a_1	Range of linearity (ppm)	r^2
Component A	1	0.475	0.961	0.3-30	0.995
	2	0.131	0.966	0.3-30	0.995
Component B	1	$-1.77\text{x}10^{-2}$	1.02	0.3-10	0.992
	2	$-2.83\text{x}10^{-2}$	0.998	0.3-10	0.992

Results

Mixture IA: 1 ppm (A), 1 ppm (B)

ppm found:	t_{d_1}	t_{d_2}
Component A	0.85	0.74
Component B	1.4	1.4
% RSD (8 replicates)	12.0%	11.7%

Mixture IB: 10 ppm (A), 10 ppm (B)

ppm found:	t_{d_1}	t_{d_2}
Component A	8.5	7.3
Component B	12	13
% RSD (8 replicates)	9.21%	8.13%

(1 Hz), the two optimum delay times yield enhancement ratios of only 1.01 and 1.02, although the total intensity changes by 50%. Thus, the requirement that the relative intensity contributions of the two components not be redundant at the two delay times is poorly met. The analysis was carried out, to see if this indeed indicates that poor results will be obtained. However, it was decided that the time required for the multiple analytical curve study would probably not produce useful data, and only one calibration curve per component was prepared (at the shorter delay time).

The results and experimental conditions appear in Table 14. The analysis can best be described as semi-quantitative (order of magnitude), except for the results on Mixture IIB. Due to the similarity of the two lifetimes, there is not enough information available from the intensity measurements to allow accurate deconvolution of the data. In addition, substantial errors are possible due to the lifetime values used in the calculations, since the lifetimes are so similar that a slight error in either could introduce large errors into the calculated component intensities. The concentration values found for component A are quite good in Mixtures IIA and IIB, but are quite low for IIC and IID. The results for component B are very low for IIA, quite good for IIB, and are high for both IIC and IID.

TABLE 14
ANALYSIS OF BINARY MIXTURE II

Component A: Thioridazine HCl $\tau = 59.6$ ms at 10 ppm

Component B: Perphenazine $\tau = 72.7$ ms at 10 ppm

$f = 1$ Hz, $t_g = 10^{-3}$s, $t_{d_1} = 5.25\text{x}10^{-2}$s, $t_{d_2} = 7.27\text{x}10^{-2}$s

486 nm, 30/70 ethanol/water

Calibration Curves (t_{d_1} only)

	a_o	a_1	Range of linearity (ppm)	r^2
Component A	−0.152	0.963	0.3−30	0.998
Component B		nonlinear		

Results

Mixture IIA: 1 ppm (A), 1 ppm (B)

ppm found:	t_{d_1}	t_{d_2}
Component A	1.3	-
Component B	0.18	-
% RSD (8 replicates)	9.61%	6.20%

Mixture IIB: 1 ppm (A), 10 ppm (B)

ppm found:	t_{d_1}	t_{d_2}
Component A	0.79	-
Component B	11	-
% RSD (8 replicates)	5.81%	3.84%

continued

TABLE 14-continued

Mixture IIC: 10 ppm (A), 1 ppm (B)

ppm found:	t_{d_1}	t_{d_2}
Component A	3.2	-
Component B	15	-
% RSD (8 replicates)	5.63%	9.32%

Mixture IID: 10 ppm (A), 10 ppm (B)

ppm found:	t_{d_1}	t_{d_2}
Component A	5.0	-
Component B	20	-
% RSD (8 replicates)	17.0%	13.0%

Ternary Mixture I

The final mixture contained three components: thioridazine HCl, with $\tau = 53.0$ ms at 30 ppm; vanillin, with $\tau = 0.264$ s at 30 ppm; and papaverine HCl, with $\tau = 2.58$ s at 30 ppm. A three component mixture had never been quantitated by the exponential method of TRP. The selection of experimental parameters is quite simple in this case. Again, a larger t_g, 10^{-3}s, is used, to decrease the OTC without affecting intensity in this lifetime range. A low frequency, 1 Hz, is required, because higher values cause the optimized response curves for vanillin and papaverine HCl to converge. Under these conditions, the three optimum delays are $t_{d_1} = 5.65\text{x}10^{-2}$s, $t_{d_2} = 0.209$ s, and $t_{d_3} = 0.455$ s. The enhancement ratios for thioridazine HCl over vanillin and papaverine HCl are 1.82 and 5.16 at t_{d_1}; for vanillin over thioridazine HCl and papaverine HCl, 3.98 and 1.54 at t_{d_2}; and for papaverine HCl over thioridazine HCl and vanillin, 170 and 1.74 at t_{d_3}. The total intensity varies by 47% from t_{d_3} to t_{d_2}, and by 30% from t_{d_2} to t_{d_1}.

The results of the analysis are presented in Table 15. The concentration values are reasonable for components A and C, but are very high for the middle component. Again, the value for the shortest lived component is most accurate at the shortest delay time. The results

TABLE 15
ANALYSIS OF TERNARY MIXTURE I

Component A: Thioridazine HCl $t = 53.0$ ms at 30 ppm

Component B: Vanillin $t = 0.264$ s at 30 ppm

Component C: Papaverine HCl $t = 2.58$ s at 30 ppm

$f = 1$ Hz, $t_g = 10^{-3}$s, $t_{d_1} = 5.65\times10^{-2}$s, $t_{d_2} = 0.209$ s, $t_{d_3} = 0.455$ s, 486 nm, 40/60 ethanol/water

Calibration Curves

	t_d	a_o	a_1	Range of linearity (ppm)	r^2
Component A	1	0.359	1.06	1-30	0.990
	2	-0.601	1.07	3-10	1.00
	3	-	-	-	-
Component B	1	-0.391	0.973	1-30	1.00
	2	-0.760	1.08	1-30	0.999
	3	-1.44	1.31	3-30	0.992
Component C	1	0.191	0.769	1-30	0.998
	2	0.176	0.754	1-30	0.998
	3	0.166	0.736	1-30	0.999

Results

Mixture IA: 10 ppm (A), 10 ppm (B), 10 ppm (C)

ppm found:	t_{d_1}	t_{d_2}	t_{d_3}
Component A	9.2	4.8	-
Component B	26	24	22
Component C	13	13	13
% RSD (16 replicates)	9.2%	9.8%	10.4%

for the intermediate component are twice the true value at all delay times. The values for the longest lived component are only slightly high, and are independent of delay time. It is reasonable to expect the accuracy of this type of analysis to suffer as the number of mixture components increases. This is due to the fact that the noise associated with the intensity of each component adds to the noise carried by every other component. Although the signal level for the mixture increases with decreasing delay time, the noise can increase. Thus, the uncertainty in the total intensity measurements can be expected to increase as the number of components increases, and this uncertainty leads to errors in the deconvolution procedure.

There are several sources of error in the preceding analyses, in addition to those discussed earlier. The primary source of error in the results for the mixture separations, other than the severe laser drift, appears to be photodecomposition of components. Although lifetime is normally concentration independent, for several solutions used in this work, decomposition was observed over the experimentation period. This was evidenced by decreased signal levels and a change in the observed lifetime. For example, over a period of several weeks, the 75 ppm vanillin solution exhibited a lifetime change of from 0.220 s to 0.284 s. Papaverine HCl showed a difference in lifetime of 2.58 s at 30 ppm, compared to 1.87 s at 46 ppm. In addition, it is not unreasonable to expect some interaction between the various mixture components, and thus altered lifetimes. Another problem that can occur is nonexponentiality of the phosphorescence decay (5, 35, 36). This occurs even in solutions of pure substances, and could be expected to occur more frequently in a mixture of phosphors. Since the exponential method of TRP requires noninteraction between components, and a very close approximation to the component lifetimes in the mixture, errors can certainly be expected if the system under study is not fairly stable and well defined.

Another source of error was the drift inherent in the amplifier and in the boxcar averager when low signal levels were being measured. The stated internally generated noise for the CW-1 is 0.10 V peak to peak (31), which could easily cause ± 10% deviation in signal levels measured for the more dilute solutions. This, coupled with DC offset drift in the second stage of the amplifier, caused uncertainties in the intensity measurements for some solutions.

CHAPTER V
CONCLUSIONS

As a result of the experimental and theoretical work presented here, a number of conclusions can be drawn with regard to time resolved phosphorimetric analysis with a pulsed source single channel gated detection system.

(i) Time resolved phosphorimetry with such a system can yield accurate quantitative analysis for spectrally similar phosphors with differing lifetimes, τ. The technique yields better results as the number of components decreases, and as the lifetime difference between the mixture components increases. The minimum lifetime difference required for resolution is estimated to be a factor of two, assuming equal SNR for the components.

(ii) The exponential method of data reduction requires more information concerning the sample system than does the MAC method, including accurate lifetimes for the individual components in the mixture. Lifetime variations in the mixture value as compared to the pure solution, due to solute-solute interactions or concentration effects, introduce significant error.

(iii) The theoretical expressions and figures presented in Chapter II correlate well with experimental results, and can be explained on a physical basis. The results can be used to optimize experimental conditions for conventional or time resolved phosphoroscopic analysis. The mixtures studied in this work were measured at experimental conditions chosen on this basis. The results indicate that the parameter values yielded adequate analyses, within the error limits introduced by the poor SNR of the measurements. For this analytical procedure to attain widespread application, both the laser flicker noise and normal immersion cooling errors must be eliminated. This might be achieved by ratioing intensity measurements to the laser output power, and by employing a conduction cooling device (37).

(iv) Calibration curves prepared at shorter delay times seem to yield better results for shorter lived components than curves prepared at longer delay times. This is apparently due to the higher signal levels present at shorter delay times. The choice of delay time seems to have little effect for longer lived components.

(v) The versatility of the experimental system, coupled with the work in Chapter II, indicate that the boxcar averager system should be applicable to a large range of TRP separations by optimizing the adjustable parameters.

(vi) In some cases, it should be possible to optimize the system response in such a manner as to render the intensity contributions from phosphors other than the analyte negligible. This would make possible direct quantitation from a single intensity measurement. This is expected to be possible only if the lifetimes of the mixture components differ greatly.

APPENDIX
THE GROWTH AND DECAY OF PHOSPHORESCENCE IN GLASSY MEDIA(29)

This Appendix contains the kinetic analysis of McGlynn, Srinivasan and Maria (29). Table A1 and Figure A1 are reproduced by permission of the publisher. Some assumptions and comments concerning the kinetic scheme are:

(i) The important events which occur during the course of irradiation of the standard type of aromatic molecule, which contains no hetero atoms, are those shown in Figure A1 and Table A1;

(ii) Direct $T_1 \leftarrow S_0$ pumping is insignificant;

(iii) T-T annihilation events are not of great importance to the T_1 population;

(iv) Intermolecular events are present implicitly, since excess energies associated with nonradiative events can be converted to heat;

(v) $S_1 \leftarrow S_0$ represents the sum total of all $S_i \leftarrow S_0$ processes, because internal conversion rapidly deactivates all higher S states to S_1.

Because the total population of molecules is conserved,

$$[N_0]=[S_0]+[S_1]+[T_1] \qquad \text{(A1)}$$

where $[N_o]$ is the total solute concentration. By defining $K_1 \equiv k_1^* + k_1$ and $K_3 \equiv k_3^* + k_3$, the rate equations for the various states are given by

$$d[S_0]/dt = -E_0[S_0] + K_1[S_1] + K_3[T_1] \qquad \text{(A2)}$$

$$d[S_1]/dt = E_0[S_0] - (K_1 + k_2)[S_1] + g_3[T_i] \qquad \text{(A3)}$$

TABLE A1
KINETIC EVENTS IN A RIGID GLASS SYSTEM CONTAINING ONE SOLUTE

Kinetic Event	Rate Constant	Comments
$S_0 + h\nu \rightarrow S_1$	E_0	Absorption
$S_1 \rightarrow S_0 + h\nu_f$	k_1^*	Fluorescence
$S_1 \rightsquigarrow S_0 + \Delta$	k_1	Nonradiative; quenching of S_1; internal conversion
$S_1 \rightsquigarrow T_1 + \Delta$	k_2	Nonradiative; quenching of S_1; intersystem crossing
$T_1 \rightarrow S_0 + h\nu_p$	k_3^*	Phosphorescence
$T_1 \rightsquigarrow S_0 + \Delta$	k_3	Nonradiative; quenching of T_1; intersystem crossing
$T_1 + h_\nu \rightarrow T_i$	g_1	Triplet-triplet absorption
$T_i \rightsquigarrow T_1$	g_2	Nonradiative; quenching of T_i; internal conversion
$T_i \rightsquigarrow S_1$	g_3	Nonradiative; quenching of T_i; intersystem crossing

Reprinted with permission from reference 29. Copyright 1971 John Wiley Sons, Inc.

Figure A1. Kinetic processes occurring during growth and decay of phosphorescence (straight arrows are radiative events, wavy arrows are nonradiative events). Reprinted with permission from reference 29. Copyright 1971 John Wiley & Sons, Inc.

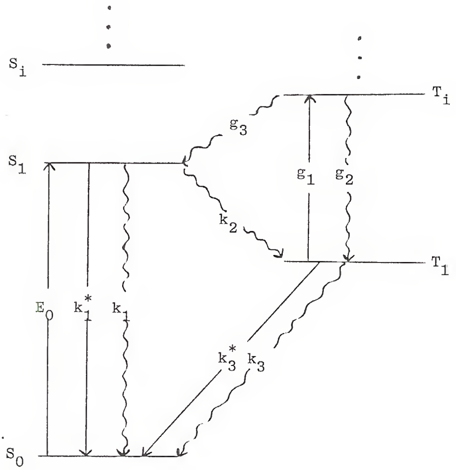
S_i
T_i
g_3
S_1
g_1
g_2
k_2
T_1
E_0
k_1^*
k_1
k_3^*
k_3
S_0

$$d[T_1]/dt = k_2[S_1] - (K_3 + g_1)[T_1] + g_2[T_i] \quad (A4)$$

$$d[T_i]/dt = g_1[T_1] - (g_2 + g_3)[T_i] \quad (A5)$$

It is reasonable to assume that $[T_i]$ populations reach steady state values rapidly, and by setting $d[T_i]/dt=0$, we obtain

$$[T_i] = g_1[T_1]/(g_2 + g_3) \quad (A6)$$

By defining $g \equiv g_1g_3/(g_2 + g_3)$, and using Equation A6, A3 and A4 can be simplified to

$$d[S_1]/dt = E_0[S_0] - (K_1 + k_2)[S_1] + g[T_1] \quad (A7)$$

$$d[T_1]/dt = k_2[S_1] - (K_3 + g)[T_1] \quad (A8)$$

The usual solution of these equations involves assuming a steady state for $[S_1]$. However, it has been shown that this is invalid, because trapping in the long-lived T_1 state can cause significant ground-state depletion. Therefore, the solution is obtained in the following fashion. Substituting S_1 from Equation A1 into Equation A8 yields

$$d[T_1]/dt = -(k_2 + k_3 + g)[T_1] - k_2[S_0] + k_2[N_0] \quad (A9)$$

This leads to a homogeneous second-order differential equation in $[T_1]$,

$$\frac{d^2[T_1]}{dt^2} + (\lambda_1 + \lambda_2)\frac{d[T_1]}{dt} + \lambda_1\lambda_2[T_1] = E_0k_2[N_0] \quad (A10)$$

where

$$\lambda_1 + \lambda_2 \equiv E_0 + K_1 + k_2 + k_3 + g \quad (A11)$$

and

$$\lambda_1\lambda_2 \equiv [(E_0 + K_1 + k_2)(K_3 + g)] + (E_0 - g) \qquad (A12)$$

Solving this gives

$$[T_1] = \frac{[N_0]E_0k_2}{\lambda_1\lambda_2}[1 - \exp(-\lambda_2 t)] \qquad (A13)$$

and

$$[S_0] = [N_0]\{1-[E_0(k_2 + K_3 + g)/\lambda_1\lambda_2][1-\exp(-\lambda_2 t)]\} \qquad (A14)$$

where

$$\lambda_2 = K_3 + g + [k_2(E_0-g)]/(E_0 + K_1 + k_2 - K_3 - g) \qquad (A15)$$

Therefore, the growth of phosphorescence occurring when the sample is subjected to constant-intensity irradiation is given by

$$\begin{aligned} I/I_0 &= 1-\exp(-\lambda_2 t) \\ &= 1-\exp(-t/\tau^R) \qquad (A16) \end{aligned}$$

where I_0 is the steady-state phosphorescence intensity and the phosphorescence growth lifetime is

$$\tau^R = 1/\lambda_2 = 1/K^R \qquad (A17)$$

The phosphorescence decay is given by

$$(I/I_0) = \exp(-K_3 t) = \exp(-t/\tau) \qquad (A18)$$

where τ is the phosphorescence decay lifetime.

The value of $[S_0]$ is obtained by assuming

$$[N_0] \simeq [S_0] + [T_1] \qquad (A19)$$

Thus, $[S_1]$ is assumed to be quite small. In addition, the validity of the steady-state approximation for $[T_i]$ assumes that the lifetime of the T_i state is 10^4 smaller than the lifetime of the S_1 state.

The rate constants for phosphorescence growth and decay thus obtained are

$$1/\tau^R = K_3 + g + [k_2(E_0 - g)]/[E_0 + K_1 + k_2 - K_3 - g] \quad \text{(A20)}$$

$$1/\tau = K_3 \quad \text{(A21)}$$

and

$$1/\tau^R - 1/\tau = g + [k_2(E_0 - g)]/(E_0 + K_1 + k_2 - K_3 - g) \quad \text{(A22)}$$

In the absence of triplet-triplet absorption, the experimentally most relevant set of equations is obtained. We find that

$$1/\tau^R = K_3 + k_2E_0/(K_1 + k_2) \quad \text{(A23)}$$

The steady-state concentration of T_1 molecules is

$$[T_1]_0 = [N_0]E_0k_2/\lambda_1\lambda_2 \quad \text{(A24)}$$

where

$$\lambda_1\lambda_2 = (K_1 + k_2)K_3 + k_2E_0 \quad \text{(A25)}$$

Combining Equations A23-A25 yields

$$[T_1]_0 = [N_0][1-(\tau^R/\tau)] \quad \text{(A26)}$$

and

$$[S_0]_0 = [N_0](\tau^R/\tau) \ . \quad \text{(A27)}$$

LIST OF REFERENCES

1. G. N. Lewis and M. Kasha, J. Am. Chem. Soc. 66, 2100 (1944).

2. R. J. Keirs, R. D. Britt and W. E. Wentworth, Anal. Chem. 28, 202 (1957).

3. T. C. O'Haver and J. D. Winefordner, Anal. Chem. 38, 602 (1966).

4. T. C. O'Haver and J. D. Winefordner, Anal. Chem. 38, 1258 (1966).

5. P. A. St. John and J. D. Winefordner, Anal. Chem. 39, 500 (1967).

6. H. C. Hollifield and J. D. Winefordner, Chemical Instrumentation 1, 341 (1969).

7. J. D. Winefordner, Acc. Chem. Res. 2, 361 (1969).

8. R. P. Fisher and J. D. Winefordner, Anal. Chem. 44, 948 (1972).

9. C. M. O'Donnell, K. F. Harbaugh, R. P. Fisher and J. D. Winefordner, Anal. Chem. 45, 609 (1973).

10. K. F. Harbaugh, C. M. O'Donnell and J. D. Winefordner, Anal. Chem. 45, 381 (1973).

11. K. F. Harbaugh, C. M. O'Donnell and J. D. Winefordner, Anal. Chem. 46, 1206 (1974).

12. R. M. Wilson and T. L. Miller, Anal. Chem. 47, 256, (1975).

13. H. B. Mark, Jr., R. M. Wilson, T. L. Miller, T. V. Atkinson, A. M. Yecynych and H. Woods In "Information Chemistry," S. Fujiwara and H. B. Mark, Jr., Eds.; University of Tokyo Press; Tokyo, Japan, 1975; pp 3-28.

14. C. M. O'Donnell and J. D. Winefordner, Clinical Chemistry 21, 285 (1975).

15. D. E. Goeringer and H. L. Pardue, Anal. Chem. 51, 1054 (1979).

16. G. M. Ridder and D. W. Margerum, Anal. Chem. 49, 2098 (1977).

17. G. E. Mieling and H. L. Pardue, Anal. Chem. 50, 1611 (1978).

18. B. G. Willis, W. H. Woodruff, J. R. Frysinger, D. W. Margerum and H. L. Pardue, Anal. Chem. 42, 1350 (1970).

19. G. D. Boutilier and J. D. Winefordner, Anal. Chem. 51, 1384 (1979).

20. J. D. Winefordner, S. G. Schulman and T. C. O'Haver "Luminescence Spectrometry in Analytical Chemistry", Wiley-Interscience: New York, 1972.

21. R. P. Fisher, Ph.D. Dissertation, University of Florida, Gainesville, Florida, 1971.

22. L. V. Hood, Ph.D. Dissertation, University of Florida, Gainesville, Florida, 1968.

23. P. A. St. John, W. J. McCarthy and J. D. Winefordner, Anal. Chem. 38, 1828 (1966).

24. M. Zander, Angew. Chem. Intern. Ed. Engl. 4, 930 (1965).

25. M. Kasha, Discussions Faraday Soc. 9, 14 (1950).

26. G. D. Boutilier, J. D. Bradshaw, S. J. Weeks and J. D. Winefordner, Applied Spectroscopy 31, 307 (1977).

27. N. Omenetto, G. D. Boutilier, S. J. Weeks, B. W. Smith and J. D. Winefordner, Anal. Chem. 49, 1076 (1977).

28. E. J. Purcell "Calculus with Analytic Geometry," 2nd ed.; Appleton-Century-Crofts; New York, 1972.

29. S. P. McGlynn, B. N. Srinivasan and H. J. Maria in "Spectrochemical Methods of Analysis," J. D. Winefordner, Ed.; Wiley-Interscience; New York, 1971; pp 285-294.

30. G. D. Boutilier, Ph.D. Dissertation, University of Florida, Gainesville, Florida, 1978.

31. "Instruction Manual: Boxcar Integrator Model CW-1," PAR Corporation; Princeton, NJ, 1969.

32. "Technical Literature: Biomac 1000 Signal Analysis Computer," Data Laboratories Limited; Mitcham, Surrey.

33. P. G. Stecher, Ed. "The Merck Index," 8th ed.; Merck and Co., Inc.; Rahway, NJ, 1968.

34. E. G. C. Clarke, Ed. "Isolation and Identification of Drugs"; The Pharmaceutical Press; London, 1969.

35. R. Rusakowicz, G. W. Byers and P. A. Leermakers, J. Am. Chem. Soc. 93, 3263 (1971).

36. R. N. Griffin, Photochem. Photobiol. 71, 159, 175 (1968).

37. J. L. Ward, G. L. Walden, R. P. Bateh and J. D. Winefordner, Appl. Spectr. 34, 348 (1980).

BIOGRAPHICAL SKETCH

Charles Glenn Barnes was born October 8, 1954, in Natchez, Mississippi. He attended elementary and secondary schools there, graduating from Adams County Christian School in May, 1972. He went to Mississippi College as a National Merit and Presidential Scholar. Mr. Barnes was an affiliate of the American Chemical Society, held membership in Phi Mu Alpha Sinfonia and Alpha Chi, and was President of the Mississippi College Circle of Omicron Delta Kappa. In addition, he served as a student representative on the College's Administrative Council, and was selected to appear in *Who's Who in American Colleges and Universities*.

Mr. Barnes served the Chemistry Department as a laboratory instructor and tutor. He was awarded the Izard Chemistry Award in 1973, a Shell Oil Corporation Science Scholarship in 1975, and the Barnhill Chemistry Award in 1976. He participated in the Chemistry Honors Program, and received the Bachelor of Science degree with Distinction and High Honors in May, 1976.

Graduate studies were begun in September, 1976, at the University of Florida, where Mr. Barnes was awarded a teaching fellowship.

I certify that I have read this study and that in my opinion it conforms to acceptable standards of scholarly presentation and is fully adequate, in scope and quality, as a dissertation for the degree of Doctor of Philosophy.

J D Winefordner

J. D. Winefordner, Chairman
Graduate Research Professor
of Chemistry

I certify that I have read this study and that in my opinion it conforms to acceptable standards of scholarly presentation and is fully adequate, in scope and quality, as a dissertation for the degree of Doctor of Philosophy.

Gerhard M. Schmid

Gerhard M. Schmid, Cochairman
Associate Professor of Chemistry

I certify that I have read this study and that in my opinion it conforms to acceptable standards of scholarly presentation and is fully adequate, in scope and quality, as a dissertation for the degree of Doctor of Philosophy.

Roger G. Bates

Roger G. Bates
Professor Emeritus of Chemistry

I certify that I have read this study and that in my opinion it conforms to acceptable standards of scholarly presentation and is fully adequate, in scope and quality, as a dissertation for the degree of Doctor of Philosophy.

George B. Butler

George B. Butler
Professor of Chemistry

I certify that I have read this study and that in my opinion it conforms to acceptable standards of scholarly presentation and is fully adequate, in scope and quality, as a dissertation for the degree of Doctor of Philosophy.

Roland C. Anderson

Roland C. Anderson
Professor of Engineering Sciences

This dissertation was submitted to the Graduate Faculty of the Department of Chemistry in the College of Liberal Arts and Sciences and to the Graduate Council, and was accepted as partial fulfillment of the requirements for the degree of Doctor of Philosophy.

December 1980

Dean, Graduate School